

# Engineering Floquet codes by rewinding

Arpit Dua,<sup>1,2,\*</sup> Nathanan Tantivasadakarn,<sup>3,1,4</sup> Joseph Sullivan,<sup>5,6</sup> and Tyler D. Ellison<sup>6,†</sup>

<sup>1</sup>*Department of Physics, California Institute of Technology, Pasadena, CA 91125, USA*

<sup>2</sup>*Institute for Quantum Information and Matter,  
California Institute of Technology, Pasadena, California 91125, USA*

<sup>3</sup>*Walter Burke Institute for Theoretical Physics, California Institute of Technology, Pasadena, CA 91125, USA*

<sup>4</sup>*Department of Physics, Harvard University, Cambridge, MA 02138, USA*

<sup>5</sup>*Stewart Blusson Quantum Matter Institute, University of British Columbia, Vancouver, BC, Canada V6T 1Z1*

<sup>6</sup>*Department of Physics, Yale University, New Haven, CT 06511, USA*

Floquet codes are a novel class of quantum error-correcting codes with dynamically generated logical qubits, which arise from a periodic schedule of non-commuting measurements. We engineer new examples of Floquet codes with measurement schedules that *rewind* during each period. The rewinding schedules are advantageous in our constructions for both obtaining a desired set of instantaneous stabilizer groups and for constructing boundaries. Our first example is a Floquet code that has instantaneous stabilizer groups that are equivalent – via finite-depth circuits – to the 2D color code and exhibits a  $\mathbb{Z}_3$  automorphism of the logical operators. Our second example is a Floquet code with instantaneous stabilizer codes that have the same topological order as the 3D toric code. This Floquet code exhibits a splitting of the topological order of the 3D toric code under the associated sequence of measurements i.e., an instantaneous stabilizer group of a single copy of 3D toric code in one round transforms into an instantaneous stabilizer group of two copies of 3D toric codes up to nonlocal stabilizers, in the following round. We further construct boundaries for this 3D code and argue that stacking it with two copies of 3D subsystem toric code allows for a transversal implementation of the logical non-Clifford  $CCZ$  gate. We also argue that the coupled-layer construction of the X-cube Floquet code can be modified by a rewinding schedule so that each of the instantaneous stabilizer codes is finite-depth-equivalent to the X-cube. Our final example is a generalization of the honeycomb code to 3D, which has instantaneous stabilizer codes with the same topological order as the 3D fermionic toric code.

## CONTENTS

I. Introduction	1
II. Rewinding Floquet code schedules	2
III. 2D Floquet color code	3
A. 3-round measurement schedule	3
B. $\mathbb{Z}_3$ automorphism of logical operators	5
C. 6-round rewinding schedule	5
IV. 3D Floquet toric code	5
A. Review: coupled layer construction	5
B. Review: 2D Floquet toric code	6
C. 6-round rewinding schedule	7
D. Boundary construction	11
E. Transversal non-Clifford gate	13
V. 3D Floquet fermionic toric code	13
A. 16-round measurement schedule	14
VI. Discussion	16
References	18
A. Rewinding X-cube Floquet code	20
B. Logical qubits of the 3D Floquet toric code	20
C. Alternative 6-round Floquet color code schedule	20

## I. INTRODUCTION

Quantum error-correcting codes are a key ingredient for fault-tolerant quantum computation. There is an active effort to develop new error-correcting codes with better code properties, such as encoding rate, code distance, and circuit-level thresholds. For every such error-correcting code, there is an associated quantum dynamics involving quantum gates, errors, and the repeated extraction of the syndrome for decoding. Naturally, the goal of developing new error-correcting codes is to optimize the quantum dynamics to reduce overheads and minimize the noise on the logical information.

Recently, Hastings and Haah introduced the first example of what has emerged as a new class of codes, dubbed Floquet codes, which exhibit dynamically generated logical qubits [1]. In their example, the dynamics of the system is governed by a periodic sequence of non-commuting 2-qubit Pauli measurements and exhibit instantaneous stabilizer codes that are a sequence of topological quantum error-correcting codes. Importantly, the schedule is such that the logical information is preserved from one instantaneous code space to the next. Given the low-weight parity checks needed to operate the code and its relatively high error threshold [2–4], Floquet codes offer compelling alternatives to the surface code. The current understanding of Floquet codes is still under active development, thus, underscoring the importance of introducing new examples and formalizing the tools to develop new Floquet codes.

In this paper, we introduce three new examples of topological Floquet codes, referred to as: (1) the Floquet color code, (2) the 3D Floquet toric code (TC), and (3) the 3D Floquet fermionic toric code (fTC). An essential tool employed in our constructions is the concept of “rewinding” a measurement schedule, where at some point within a period, the sequence of measurements is reversed. A similar strategy was used in Ref. [5] to adapt the honeycomb code to a system with boundary. We further use rewinding in this work to ensure that the ISGs are characterized by a desired topological order and to avoid inadvertently measuring logical operators.

(1) Our first example is the Floquet color code, which exhibits instantaneous stabilizer groups (ISGs) that are equivalent under a finite-depth local quantum circuit with ancilla (FDLQC-equivalent) to the 2D color code. This should not be confused with the CSS honeycomb code of Refs. [6–8], which is also referred to as the Floquet color code in Ref. [7]<sup>1</sup>. We consider two different measurement schedules for the Floquet color code. The first exhibits an order three automorphism of the logical operators, while the second is a rewound version with a trivial automorphism – in principle enabling the construction of boundaries. Notably, one of the ISGs is equivalent to the conventional color code up to concatenation with a 3-qubit repetition code – thus allowing for the transversal implementation of certain logical Clifford gates.

(2) Our second example is the 3D Floquet TC, which has ISGs that are FDLQC-equivalent to the usual 3D TC (or two copies of it). Our construction is inspired by the coupled layer construction of Ref. [9], in the sense that we prepare an instantaneous state of stacks of 2D TCs along orthogonal directions, then perform measurements that “condense” pairs of  $e$  anyons along the intersection of two orthogonal layers. In the subsequent rounds of measurements, the stabilizers responsible for the condensation generically evolve into higher-weight stabilizers. By making use of a schedule that rewinds, we ensure that the system does not evolve back into a stack of 2D TCs.

We note that the construction of the X-cube Floquet code in Ref. [10] similarly uses a coupled layer construction. However, in their construction, the ISGs evolve back into decoupled layers of 2D TCs (up to nonlocal stabilizers). We point out in Appendix A that this can be avoided by rewinding the schedule. We also note that Ref. [11] presents a construction of a 3D Floquet toric code using the path-integral framework.

Due to the evolution of condensation terms into higher-weight operators, we observe an exotic splitting of the 3D TC ISG obtained in the preceding round to two copies of 3D TC up to nonlocal stabilizers. We also construct a planar variant of the 3D Floquet TC which has boundaries that condense point-like or loop-like excitations for each ISG. Unlike the planar variant of the 2D Floquet

TC, the boundaries of the 3D Floquet TC do not undergo an automorphism. By stacking this planar variant of the 3D Floquet TC with two copies of the planar variant of “subsystem toric code” [12] (with 3-qubit checks), we can prepare an instantaneous state of cubic lattice 3D TC stacked with two copies of 3D checkerboard lattice TC. Such a stacked code allows for an implementation of the logical non-Clifford  $CCZ$  gate [13, 21].

(3) Lastly, we construct a Floquet code with ISGs that are FDLQC-equivalent to the 3D fermionic TC, i.e., with the same topological order as a 3D  $\mathbb{Z}_2$  gauge theory with an emergent fermion [14]. Our construction is based on the 3D generalization of Kitaev’s honeycomb model of Ref. [15]. In this construction, we use rewinding to avoid inadvertently measuring logical operators throughout the schedule.

Our work establishes new examples of Floquet codes and formalizes rewinding as a tool for designing Floquet codes with beneficial code properties, such as transversal logical gates. We expect that constructing examples such as these will be an important step towards developing a more comprehensive classification and characterization of Floquet codes.

The paper is organized as follows. In Sec. IV, we review the Floquet code of Ref. [4], referred to as the Floquet TC, and state general properties of rewinding schedules – such as trivial logical automorphisms after a measurement cycle. In Secs. III, IV, and V, we define the Floquet color code, the 3D Floquet TC, and the 3D Floquet fTC, respectively.

## II. REWINDING FLOQUET CODE SCHEDULES

In this section, we formalize the notion of a rewinding measurement schedule for a Floquet code. We argue that a Floquet code with a rewinding schedule exhibits a trivial automorphism of the logical operators after a single period and that the measurement quantum cellular automata (MQCAs) defined at the boundary have a trivial index [16]. We begin with some preliminary definitions.

### 1. Preliminaries

In general, a Floquet code is defined by two pieces of data: (i) a set of operators that are measured throughout the dynamics, known as the check operators (or more simply, the checks), and (ii) a periodic measurement schedule, which dictates when the check operators should be measured. We find it convenient to further define the check group as the group generated by the checks. We call the center of the check group, i.e., the subgroup of operators in the check group which commute with every element of the check group, the stabilizer group of the check group. We note that the stabilizers can be interpreted as conserved quantities of the dynamics since their

<sup>1</sup> In contrast to our Floquet color code, the ISGs of the CSS honeycomb code are FDLQC-equivalent to the 2D TC.

measurement outcomes are not affected by the measurement of the checks.

We say that a measurement schedule rewinds, or that the Floquet code is a rewinding Floquet code, if the sequence of measurements are performed in reverse order at some point in the schedule. For example, we consider a set of measurements labeled 0, 1, and 2. If the measurements are performed periodically in the sequence 012021, as in Ref. [5], then the schedule is in fact rewinding. This can be seen by writing a few periods of the schedule as:

$$\dots 0120-0210-0120-0210-0120-0210\dots, \quad (1)$$

where we have inserted repetitions of the 0 measurements. The sequence 0120 is then explicitly followed by the reverse sequence 0210. In our examples below, we find that rewinding is a useful tool for constructing Floquet codes with a desired set of ISGs and to construct boundaries, as acknowledged in Refs. [3–5]. This may in turn be useful for developing Floquet codes with beneficial decoding properties and transversal implementations of logical gates.

## 2. Trivial automorphism and MQCA index

We now state the general properties of such rewinding schedules – specifically, we emphasize that there is a trivial automorphism of the logical operators, implying that a planar variant of the rewinding Floquet code defines a measurement quantum cellular automata at its boundary with a trivial index [16, 17].

Consider a Floquet code with a rewinding schedule of form 012021 on a torus. We assume that this Floquet code is reversible in the sense of Ref. [16]. This means that for each consecutive pair of ISGs, there exist a complete set of shared logical operator representations for every logical operator. That is, there is a complete set of operators that commute with both stabilizer groups. In between rounds, we must update the logical operators by multiplying instantaneous stabilizers of the current round, to obtain a logical that also commutes with the ISG of the next round. Intuitively speaking, the rewinding ensures that any instantaneous stabilizers that were multiplied to the logical operators are removed when the schedule is run backwards. Thus, we arrive back at the same logical representative after the full rewind cycle.

To see this explicitly, we denote the representations of a logical operator that are shared by ISGs of consecutive rounds  $r$  and  $r'$  as  $\text{LOR}(r, r')$  where round  $r'$  follows round  $r$ . For the 6-round schedule 012021, the logical operator representations of rounds 0 and 1 can be chosen to be  $\text{LOR}(0, 1)$ . To evolve to round 2, we can multiply by instantaneous stabilizers of the 1-ISG to obtain  $\text{LOR}(1, 2)$ . To go to the second instance of round 0, we can multiply by instantaneous stabilizers of the 2-ISG to obtain  $\text{LOR}(2, 0)$ . We now begin the rewinding process.  $\text{LOR}(2, 0) = \text{LOR}(0, 2)$  is a valid representation for the second instance of round 2. The next rounds are 1 and

0 so we multiply by the same elements of the 2-ISG to obtain  $\text{LOR}(2, 1)$  and the same elements of the 1-ISG to obtain  $\text{LOR}(1, 0) = \text{LOR}(0, 1)$ . The net result is that we are back to the original representation  $\text{LOR}(0, 1)$  that we started with. Hence, the automorphism is trivial. Later in Sec. IV B, we explicitly show the shared logical operators for the rewinding sequence of the 2D Floquet TC in Fig. 3.

The argument that the logical operators “rewind” also implies that the MQCA, as defined in Ref. [16], is trivial. If the Floquet code is put on a system with a boundary, one can consider the evolution of the logical operators at the boundary as defining an MQCA. Then, since the automorphism of logical operator representations is trivial, the MQCA is also trivial.

## III. 2D FLOQUET COLOR CODE

In this section, we construct the 2D Floquet color code, whose ISGs are FDLQC-equivalent to the 2D color code. We then discuss the  $\mathbb{Z}_3$  automorphism of logical operators and the construction of a rewinding schedule that trivializes the automorphism.

The Floquet color code is based on the topological subsystem code of Ref. [18], which is defined on the ruby lattice with a qubit at each vertex, as depicted in Fig. 1(a). The group of check operators is generated by two-qubit operators, specified by assigning a label  $x$ ,  $y$ , or  $z$  to each edge of the lattice. The corresponding check operators on the  $x$ -,  $y$ -, and  $z$ -edges are the two-qubit Pauli operators,  $XX$ ,  $YY$ , and  $ZZ$ , respectively.<sup>2</sup>

The stabilizers of the check group are generated by two types of operators, both of which can be supported on an “inflated” hexagon of the ruby lattice, as shown in Fig. 1(a). We call the generator that is a product of  $Z$  operators around a hexagon the hexagon stabilizer and the generator that is a product of  $X$  and  $Y$  operators the inflated hexagon stabilizer.

### A. 3-round measurement schedule

The measurement schedule of the Floquet color code consists of three rounds, labeled by 0, 1, and 2, with the checks of each round shown in Fig. 1(b). We note that this schedule is also given in Ref. [19] in the context of the topological subsystem code.<sup>3</sup> This schedule ensures

<sup>2</sup> Through out this paper, we omit the tensor product between the Pauli operators for simplicity of notation. For example, we write  $X \otimes X$  as  $XX$ .

<sup>3</sup> Although the schedule has appeared before in the literature, here, we view the code as a Floquet code. The important difference is that the Floquet code has dynamically generated logical qubits in addition to the logical qubits of the subsystem code.

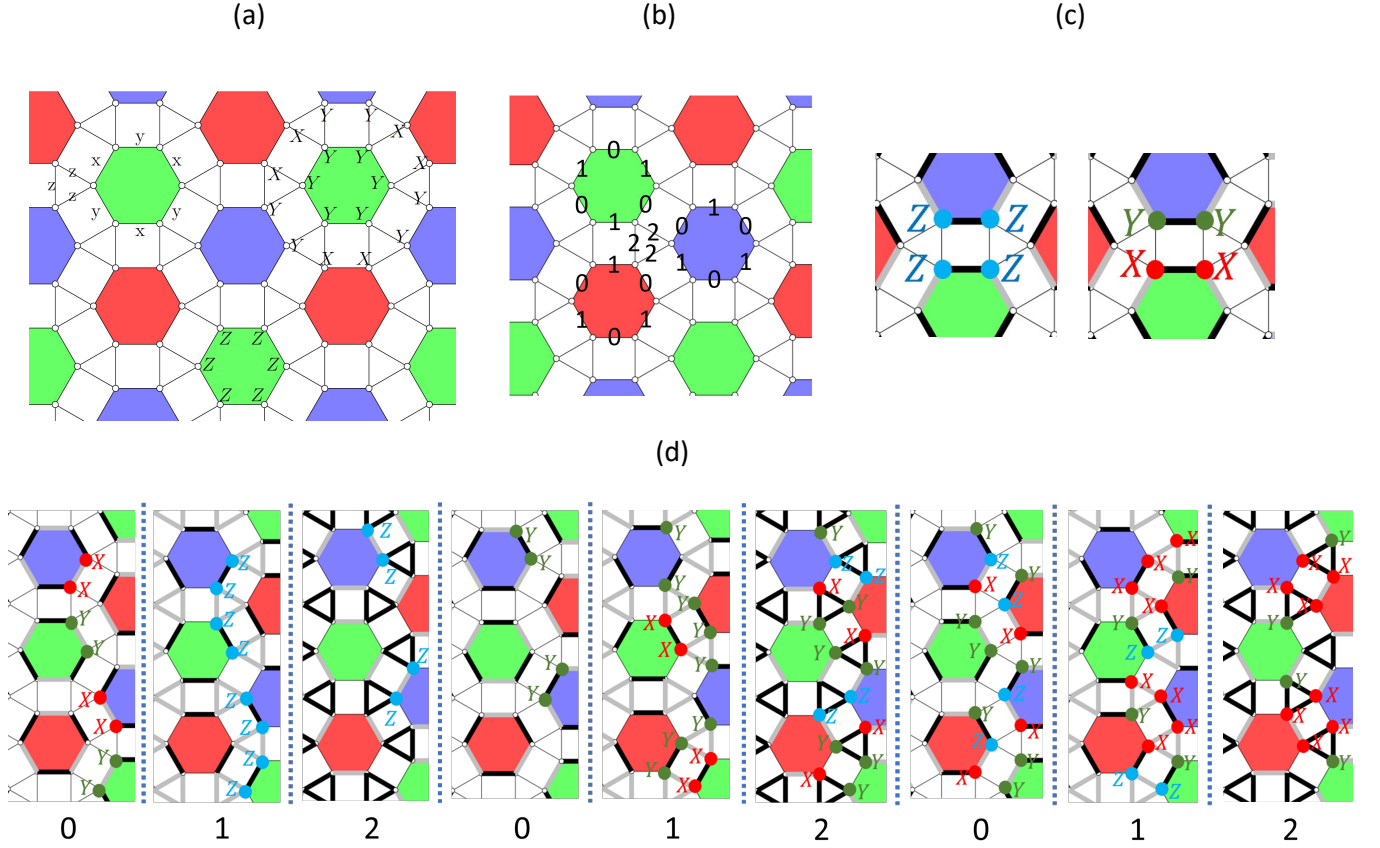


FIG. 1. (a) The ruby lattice on which the Floquet color code is defined. The edges of the hexagon are labeled as  $x$  and  $y$ , which correspond to the  $XX$  and  $YY$  check operators. All the edges connecting different colored hexagons are labeled as  $z$  corresponding to a  $ZZ$  check operator. The generators of the stabilizer group consist of two operators supported on every “inflated” hexagon. We show the two generators on two green inflated hexagons on the right. (b) The 3-round schedule of measurements of Floquet color code; all the checks on the triangle are measured in round-2 but only some are shown for clarity. (c) Instantaneous square stabilizers in rounds 0 and 1 that form from products of checks in preceding rounds. These square stabilizers are significant in the measurement of the stabilizers on the green inflated hexagon and in working out the automorphism of logical string operators. In (c) and (d), the checks of the current round are shown in black and the checks of the next round are shown in gray. (d)  $\mathbb{Z}_3$  automorphism of dynamically generated logical operators of the Floquet color code.

that the stabilizers of the check group are inferred once every cycle.

In each round, the ISG is FDLQC-equivalent to the color code. We demonstrate this for round 2, by showing that the ISG is precisely the color code concatenated with the 3-qubit repetition code. In round 2, the checks consist of  $ZZ$  operators on every edge of the triangles. Since there are three qubits and two independent checks per triangle, an effective qubit (3-qubit repetition code) lives on each triangle with effective Pauli operators

$$X_{\text{eff}} = XYY \equiv XXX \quad Z_{\text{eff}} = ZII \equiv ZZZ \quad (2)$$

where  $\equiv$  is the equivalence up to the 2-qubit  $ZZ$  checks. In terms of the effective Pauli operators, the instantaneous stabilizers reduce to those of the color code. Therefore, the round-2 ISG is the color code up to concatenation with 3-qubit repetition codes. For rounds 0 and 2, the FDLQCs that map the ISGs to the color code are given in the `Mathematica` file.

As an aside, the logical gates that can be implemented transversally for the (CSS) color code [20, 21], can still be implemented transversally in round 2 when the ISG is the color code up to concatenation with 3-qubit repetition codes. If we label the four logical qubits 1 through 4, then the transversal logical gates for a single copy of color code (in particular choice of basis) are  $\text{CNOT}_{12}\text{CNOT}_{34}$  and  $\text{SWAP}_{12}\text{SWAP}_{34}$ . To realize the former, we act with  $S_{\text{eff}} = SII$  on one orientation of triangles (say, left-pointing) and  $S_{\text{eff}}^\dagger = S^\dagger II$  on the other orientation (right-pointing) after the second round of measurements. Similarly, we can act with an effective Hadamard gate  $H_{\text{eff}} = (X_{\text{eff}} + Z_{\text{eff}})/\sqrt{2}$  on all triangles to realize the latter logical gate.

Since the logical information is preserved under the Floquet code dynamics, these gates can be done in round-2 and the processed logical information carries over to subsequent rounds. We note that a planar realization of the color code would allow for a transversal implemen-



tation of all logical Clifford gates [21, 22]. We leave the construction of a planar variant of our Floquet color code to future work.

### B. $\mathbb{Z}_3$ automorphism of logical operators

Given that the ISGs are FDLQC-equivalent to the color code, the Floquet color code encodes four logical qubits on a torus. This implies that the Floquet code has two dynamically generated logical qubits, since the topological subsystem code of Ref. [18] hosts only two logical qubits. We refer to the logical operators of the subsystem code as the static logical operators and the logical operators that are not static as the dynamically generated logical operators<sup>4</sup>. Indeed, since the static logical operators have representations that commute with all of the check operators, they do not evolve under the dynamics. As discussed below, there is a nontrivial automorphism of the logical operators after a period. This means that a subset of the dynamically generated logical operators belong to the check group but do not commute with all the elements of the check group. This is in contrast to the Floquet TC, where the dynamically generated logical operator belongs to the center of the check group.

For the 3-round Floquet cycle, the dynamically generated logical operators exhibit a  $\mathbb{Z}_3$  automorphism, as shown in Fig. 1(d). The logical operator representation in each round  $r$  commutes with the ISGs of rounds  $r$  and  $r+1$ . The logical operator representation in each round  $r$  is related to the one in the preceding round  $r-1$  via multiplication with the ISG stabilizers of round  $r$ . Besides the checks measured in round  $r$ , we used the instantaneous square stabilizers shown in Fig. 1(c) to work out the representations. Since there are no nonlocal stabilizer generators of the check group, the automorphism occurs due to multiplication with products of dynamically generated logical operators belonging to the check group. Due to the  $\mathbb{Z}_3$  automorphism that occurs every 3 rounds, it naively takes 9 rounds for a trivial automorphism.

To see the automorphism explicitly, we can apply the mapping to effective qubits in round 2 (Eq. (2)) to the string operators shown in Fig. 1(d). In the first instance of round 2, we find that the logical consists of  $Z_{\text{eff}} = ZII$  on each triangle connecting the red plaquettes. If we truncate such a string in the effective color code pictures, the  $X$  and  $Y$  red plaquettes of the effective color code will be violated. In the second instance of round 2, we have a string of  $X_{\text{eff}} = XYY$  on each triangle connecting blue plaquettes. Thus, truncating such a string will violate the  $Y$  and  $Z$  blue plaquettes of the effective color code.

Lastly, in the third instance of round 2, the strings are a product of  $Y_{\text{eff}} = XXY$  connecting green plaquettes. Truncating these strings will violate the  $X$  and  $Z$  green plaquettes of the effective color code.

### C. 6-round rewinding schedule

Instead of trivializing the automorphism through 9 measurement rounds, we can use the 6-round rewinding schedule 012102, in which the  $\mathbb{Z}_3$  automorphism action after 012 is rewound back. The evolution of logical operator representations is the same as shown in Fig. 1(c) for any three consecutive rounds with 0-, 1- and 2-checks. In principle, this rewinding schedule enables the construction of the Floquet color code on a triangular geometry, such as in Refs. [21, 22]. In the appendix, we write a different 6-round schedule for the Floquet color code, which exhibits a trivial automorphism. It would be interesting to see if that 6-round schedule is equivalent to the above rewinding schedule using some notion of equivalence, such as simple equivalence discussed in Ref. [16].

## IV. 3D FLOQUET TORIC CODE

We now present the 3D Floquet TC whose ISGs are FDLQC-equivalent to the usual 3D TC (or two copies). The construction is inspired by the coupled layer construction of the 3D TC presented in Ref. [9]. More specifically, our strategy for building the 3D Floquet TC is to start with layers of 2D Floquet codes and add measurements that implement the condensation procedure of Ref. [9] at the level of the ISGs. We use 2D Floquet codes on square-octagon lattices, which are stacked along the  $x$ -,  $y$ -, and  $z$ -axes, as our building blocks.

Before going into the detailed construction of the 3D Floquet TC, we review the coupled layer construction of the 3D TC and the construction of the 2D Floquet TC with a rewinding schedule on the square octagon lattice. Readers who are familiar with the details of the coupled layer construction of 3D TC and the 2D Floquet TC are welcome to skip directly to Sec. IV C.

### A. Review: coupled layer construction

The coupled layer construction of the 3D TC in Ref. [9] starts with stacks of 2D TCs, along the  $x$ -,  $y$ -, and  $z$ -axes, as shown in Fig. 2(a). The 2D TCs here are defined on square lattices with qubits on the edges. Taken together, the layers of 2D TCs define a cubic lattice with two qubits on each edge. The edges parallel to the  $z$ -axis, for example, have one qubit from a 2D TC in a  $yz$ -plane and another from a 2D TC in an  $xz$ -plane.

The 2D layers are then coupled together by forcing the

<sup>4</sup> The static subsystem code is characterized by the 3-fermion anyon theory [23–26], thus, the dynamically generated logical operators are associated with a second copy of the 3-fermion theory. The two 3-fermion theories together are equivalent to the color code.

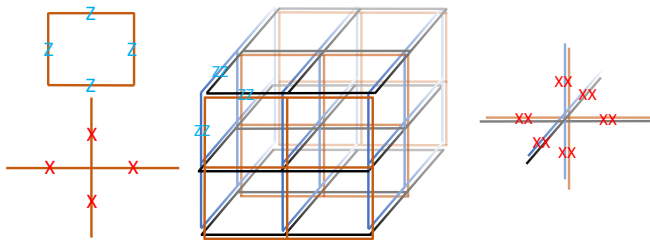


FIG. 2. Constructing three-dimensional topological codes from stacks of 2D TCs. Stacks of 2D TCs along three orthogonal directions. A choice of vertex and plaquette stabilizers in each 2D TC layer of the stacks is shown on the left. Putting the three orthogonal stacks of 2D TC stacks together results in a lattice where each edge is now a composite edge that consists of two edges (qubits) from the 2D TC layers. Measuring  $ZZ$  on the pair of qubits on each composite edge results in effective 3D TC stabilizers with an effective qubit (due to the  $ZZ$  stabilizer) on each composite edge; some  $ZZ$  stabilizers on the composite edges are shown. The resulting  $X$ -stabilizer is shown on the right. Measuring  $XX$  instead of  $ZZ$  on the pair of qubits on each composite edge results in the  $X$ -cube model stabilizers on the effective qubits.

interlayer  $ZZ$  operator at each edge to be a stabilizer.<sup>5</sup> This requires removing the 2D TC stabilizers that fail to commute with the  $ZZ$  operators. Note that the vertex terms of the 2D TCs do not commute with the interlayer  $ZZ$  checks, but the product of three vertex stabilizers, one from each intersecting plane, does commute. Therefore, this product of  $X$ -type stabilizers remains in the stabilizer group.

Operationally, the  $ZZ$  stabilizers define a single effective qubit at each edge. The effective stabilizer group is then equivalent to the usual 3D TC up to concatenation with two-qubit repetition codes; the product of three vertex stabilizers becomes the vertex stabilizer on the cubic lattice and the plaquette interlayer  $ZZ$  checks, the logical operators of the 3D TC can be represented by  $e$  string operators along non-contractible paths and membranes built from stacks of  $m$  string operators.

Intuitively, the interlayer  $ZZ$  operators create pairs of  $e$  anyons. By adding the  $ZZ$  operators to the stabilizer group, we have condensed pairs of  $e$  anyons from intersecting 2D TCs. Along the  $z$ -axis, for example, the  $ZZ$  operator creates a pair of  $e$  anyons with one from the  $yz$ -plane and the other from the  $xz$ -plane. Heuristically, the condensation of interlayer pairs of  $e$  anyons implies that the  $e$  anyons can transfer between layers at an intersection, while the  $m$  anyons in individual layers become confined.

<sup>5</sup> We remark that if the 2D TC layers are coupled together by an interlayer  $XX$  stabilizer at each edge, then we obtain an effective  $X$ -cube model [9]. This is because the  $Z$ -type stabilizers that remain in the stabilizer group are the products of 2D TC plaquette stabilizers around a cube, corresponding to the cube-term of the  $X$ -cube model. This is used to build an  $X$ -cube Floquet code in Ref. [10]

## B. Review: 2D Floquet toric code

We now review the 2D Floquet toric code, which is essential to our 3D construction. Following Ref. [4], the 2D Floquet TC can be defined on a two-dimensional square-octagon lattice with periodic boundary conditions and a qubit at each vertex. We color the edges of the lattice red, green, and blue, as shown in Fig. 3. The red, green, and blue colors determine the 2-qubit Pauli check operators  $XX$ ,  $YY$ , or  $ZZ$ , respectively, associated to an edge. We refer to the checks on the red, green, and blue edges as  $R$ -,  $G$ -, and  $B$ -checks, respectively. The stabilizers of the check group are generated by three types of operators, supported on either a square or an octagon, as shown in Fig. 3(a). We refer to these as the square stabilizers and the octagon stabilizers.

To initialize the code, we measure the checks  $RBGR$  in sequence. Subsequently, in each period, we measure the sequence  $GBRBRG$ . As it is important in the construction of the 3D Floquet TC, we note that this schedule is rewinding, to the logical automorphism is trivial. We also note that this is the schedule used in Refs. [4] and [3] to define the 2D Floquet TC on a system with a boundary.

The ISGs immediately after measuring the  $R$ -,  $G$ -, and  $B$ -checks are referred to as the  $R$ -,  $G$ -, and  $B$ -ISGs. These ISGs are generated by the stabilizers of the check group and the corresponding set of check operators. The  $G$ -ISG, for example, is generated by the square and octagon stabilizers as well as the two-qubit  $YY$  stabilizers on the green edges.

The  $G$ -ISG is equivalent to the 2D TC on the square lattice concatenated with a 2-qubit repetition code on the green edges. More specifically, the 2-qubit repetition code on each green edge is defined by a  $YY$  stabilizer and logical operators

$$X_{\text{eff}} = XX \equiv ZZ, \quad Z_{\text{eff}} = YI \equiv IY. \quad (3)$$

That is, in the subspace where all the green checks  $YY$  are satisfied, we may define an effective qubit on each edge according to the above equation. In this subspace, the octagon stabilizers can be recast as products of  $X_{\text{eff}}$ 's on four effective qubits, allowing them to be interpreted as the vertex terms of the square lattice 2D TC. Similarly, the square stabilizers can be written as a product of  $Z_{\text{eff}}$ 's on four effective qubits and hence correspond to the plaquette terms of the 2D TC. We define the violations of vertex and plaquette stabilizers to be  $e$  anyons and  $m$  anyons, respectively. The  $e$  anyons are created by the application of  $X_{\text{eff}}$  on the green edges and the  $m$  anyons are created by the application of  $Z_{\text{eff}}$  on the green edges.

The  $R$ - and  $B$ -ISGs are equivalent to the toric code on a rotated lattice up to concatenation with a 4-qubit code. Since the  $B$ - and  $R$ -ISGs are symmetric, we make this explicit for the  $B$ -ISG. Each square of the lattice consists of four qubits and three instantaneous stabilizers, i.e., one  $YYYY$  stabilizer and an additional two  $ZZ$  stabilizers from the measurements of the  $B$ -checks. If we set the

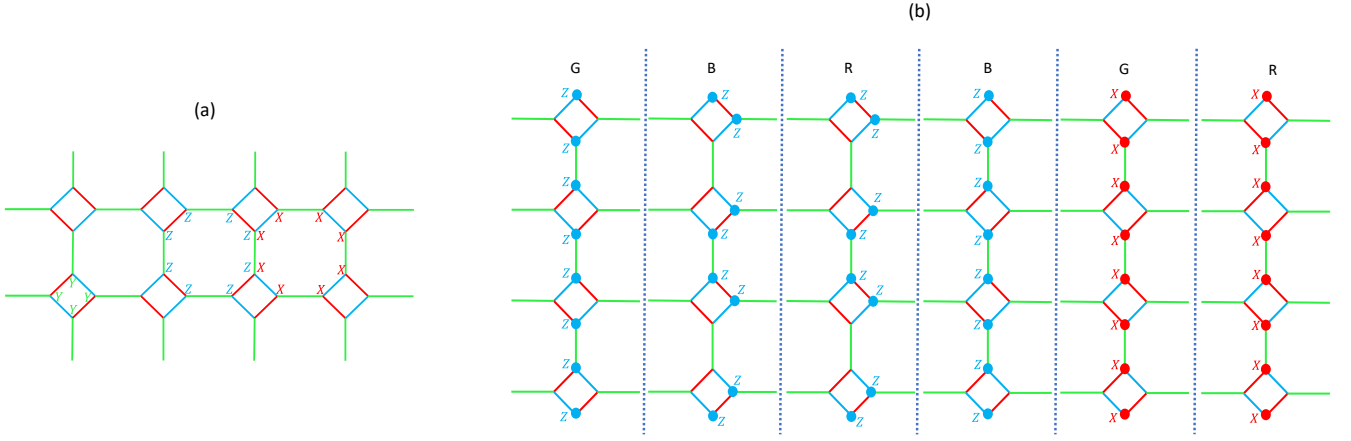


FIG. 3. (a) The check operators of the Floquet code consist of two-body Pauli check operators  $XX$ ,  $YY$ , and  $ZZ$  for the red, green, and blue edges respectively. The stabilizers of the check group are generated by the products of check operators along closed loops as shown; the product of check operators around a square plaquette consists of Pauli operators  $Y$ s while the products of check operators around octagon plaquettes consist of Pauli operators  $X$  or  $Z$  depending on the sublattice. (b) Evolution of a representation of a logical operator in the GBRBGR schedule on the square-octagon lattice. The labels at the top indicate the rounds of the Floquet code. In each round, the representations commute with both the checks of the current and of the next round. At the end of the cycle of 6 rounds, the representation is back to the starting representation and hence, the automorphism is trivial.

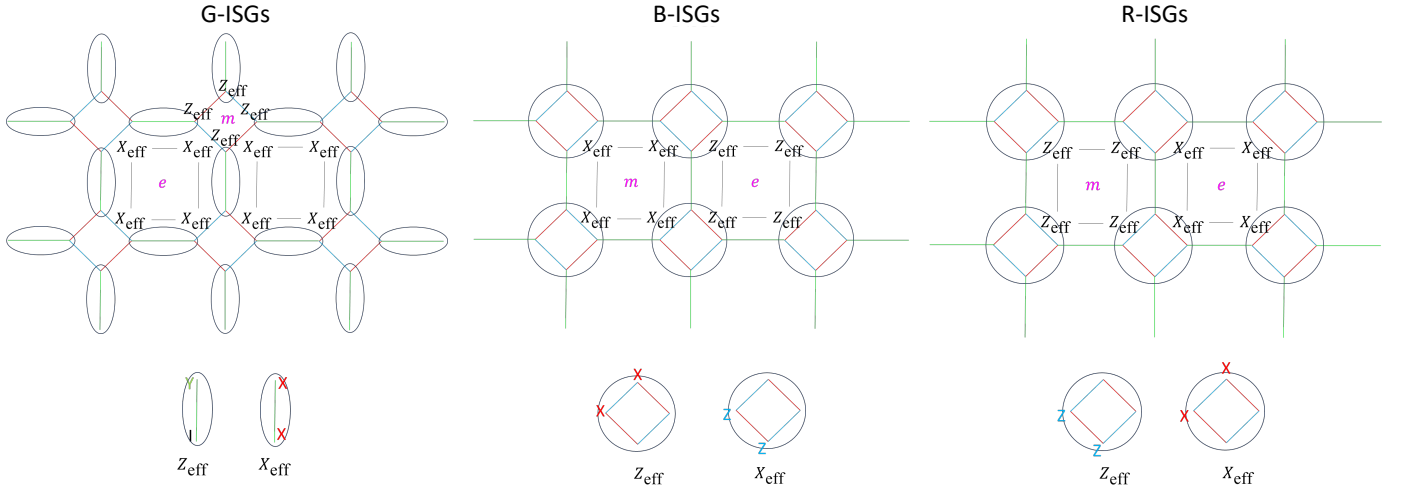


FIG. 4. Bulk stabilizers of the effective TC ISGs in the 2D Floquet code on a torus. In the G-ISGs, the effective qubits (shown using ellipses) live on the green edges and we get the usual square lattice TC stabilizers. In the B- and R-rounds, the effective qubits (shown using circles) live on the square plaquettes and we get ISGs that are 2D TCs on rotated square lattices.

above stabilizers to one, we define an effective qubit for each square as

$$X_{\text{eff}} = ZIZI, \quad Z_{\text{eff}} = XXII, \quad (4)$$

where the first two and last two qubits correspond to separate blue edges. The above operators commute with the three instantaneous stabilizers at the square. In other words, each square supports a  $[[4,1,2]]$  code. In the logical subspace of the  $[[4,1,2]]$ , the octagon stabilizers reduce to a product  $X_{\text{eff}}^{\otimes 4}$  or  $Z_{\text{eff}}^{\otimes 4}$  depending on the sublattice, as shown in Fig. 4. Thus, on the effective qubits defined by the  $[[4,1,2]]$ , we have a 2D rotated TC.

### C. 6-round rewinding schedule

To build the 3D Floquet TC, we start with layers of 2D Floquet TCs on square-octagon lattices, which are stacked along the  $x$ -,  $y$ -, and  $z$ -axes. The stacks of square-octagon lattices define a 3D truncated cubic lattice with two qubits at each vertex, see also Ref. [10]. For clarity, we resolve the vertices in Fig. 5 to show the connectivity of each square-octagon foliation.

The check group of the 3D Floquet TC is generated by the check operators of the 2D Floquet TCs and 2-qubit interlayer  $YY$  check operators that couple the layers together as in Fig. 5. There are three interlayer  $YY$  checks

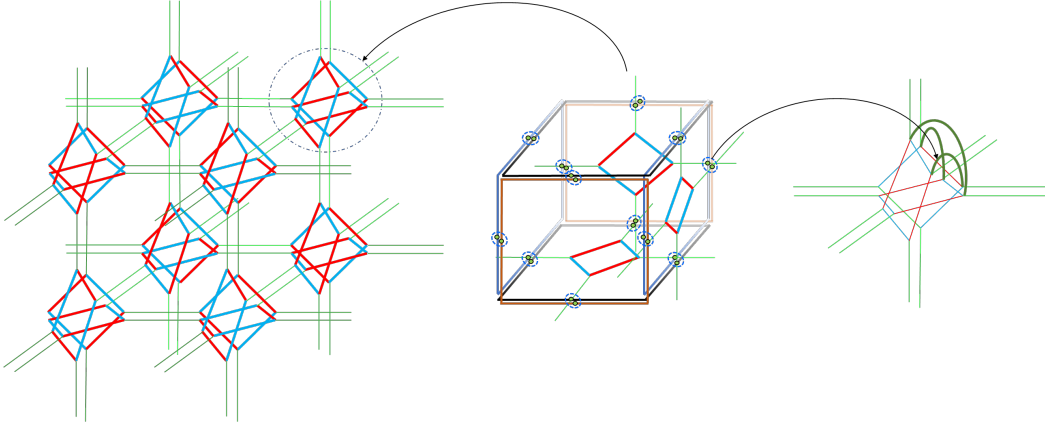


FIG. 5. Stacks of square-octagon lattice (see Fig. 3) along 3-orthogonal directions to prepare the resource stacks of 2D TC layers before reaching the 3D TC instantaneous stabilizer group (ISG) of the 3D Floquet TC. For the 3D TC ISG in round-3 (see table I), the plaquette operators on the octahedron map to the plaquette operators on the cubic lattice in the manner as shown. In the middle, we show how the plaquette stabilizers on the circled “octahedron” in the ISG of green check measurements are mapped from the plaquette stabilizers of the square lattice 2D TC layers. On the right are shown the condensation operators that couple the stacks of square-octagon models such that the resulting ISG in round-3 is the usual representation of the 3D TC on the cubic lattice in terms of the effective qubit Pauli operators.

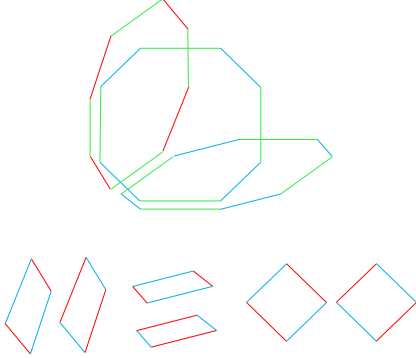


FIG. 6. Stabilizers of the check group of the 3D Floquet TC. They form a subgroup of the stabilizers of the square-octagon layers such that they commute with the condensation checks. Top: in each cube, the product of three octagon stabilizers from orthogonal foliations as shown commutes with the condensation checks. Note that the octahedrons can have four different configurations of bonds in the unit cell shown in Fig. 5, so the three octagon stabilizers that form the products may not look exactly as shown. Bottom: the square stabilizer terms from the square-octagon layers commute with the condensation checks.

for each octahedron of the truncated cubic lattice. These correspond to the three ways of pairing the  $xy$ -,  $yz$ -, and  $xz$ -planes. The stabilizers of the check group are generated by the square stabilizers of the 2D Floquet TCs and a product of three octagon stabilizers sharing a truncated cube, as in Fig. 6.

To initialize the 3D Floquet TC, we first initialize the stack of 2D Floquet codes with the four-round measurement sequence: RBGR. Afterwards, the ISG is equivalent to a stack of 2D TCs, up to concatenation with two-qubit repetition codes. We then measure the G-checks and the interlayer  $YY$  checks simultaneously (round 0 listed in

Round index	Measurement	ISG
0	G (Green $YY$ + interlayer $YY$ )	3D TC
1	B (Blue $ZZ$ )	3D TC $\times$ 3D TC
2	R (Red $XX$ )	3D TC $\times$ 3D TC
3	B (Blue $ZZ$ )	3D TC $\times$ 3D TC
4	G (Green $YY$ + interlayer $YY$ )	3D TC
5	R (Red $XX$ )	3D TC $\times$ 3D TC

TABLE I. The GBRBGR schedule of measurements for the 3D Floquet TC. The measured checks and the instantaneous stabilizer groups (ISGs) in each round are written. We note that in the ISG with two copies of 3D TC, the two copies are in an entangled logical state due to nonlocal stabilizers of the form  $\bar{Z}_{1,i}\bar{Z}_{2,i}$  where  $\bar{Z}_{1,i}$  and  $\bar{Z}_{2,i}$  are logical string operators of the two 3D TCs along nontrivial cycles  $i$  of the associated 3D tori.

Table I). In terms of the effective Pauli operators  $X_{\text{eff}}$  and  $Z_{\text{eff}}$  in the G-ISG of the 2D Floquet TC [Eq. (3)], the interlayer  $YY$  checks are precisely the  $Z_{\text{eff}}Z_{\text{eff}}$  terms of the coupled layer construction in Ref. [9]. This is to say that the interlayer  $YY$  checks create pairs of  $e$  anyons on intersecting layers. Therefore, the interlayer  $YY$  checks condense pairs of  $e$  anyons, and after measuring the  $YY$  checks, the ISG is the 3D TC, up to concatenation with 2-qubit repetition codes on the green edges.

We continue with a periodic measurement schedule of the checks, according to the sequence: GBRBGR, where the G round implicitly includes the interlayer  $YY$  checks. We note that the interlayer  $YY$  checks fail to commute with the subsequent B- and R-checks, so they are later removed from the ISG. However, products of the interlayer  $YY$  checks and instantaneous stabilizers commute with the B- and R-checks. We refer to these new instan-



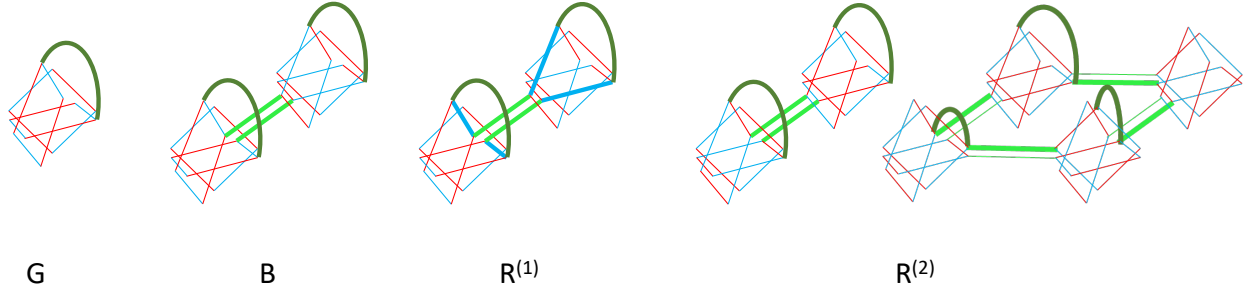


FIG. 7. The evolution of one condensation operator in the 3D Floquet toric code with schedule  $\text{GBR}^{(1)}\text{BGR}^{(2)}$  where we have added the superscripts to the R-rounds to specify their position. The different rounds are labeled. There is no difference in the ISGs in the two B-rounds and in the two G-rounds respectively due to rewinding. In G-rounds, the condensation operator is a two-qubit operator. In B-rounds, the interlayer term that survives is a product of green edges (thickened) and two original two-qubit condensation operators. Blue checks are multiplied by the representation in the B-round to get the representation in the  $\text{R}^{(1)}$ -round. In  $\text{R}^{(2)}$ -round we get a representation of the evolved condensation operator similar to the B-round but across different octahedrons. We get another interlayer term in the  $\text{R}^{(2)}$ -round which is a product of green checks and 2-qubit condensation checks of the G-round.

taneous stabilizers as the evolved condensation terms. On each octahedron of the truncated cubic lattice, only one of the three interlayer  $YY$  checks (depending on the octahedron) evolves to a constant-weight stabilizer. They are shown in Fig. 7. The other two evolve into nonlocal stabilizers.

The generators of each of the ISGs thus consist of (i) the checks measured in that round, (ii) the condensation operators or evolved condensation operators, (iii) octagon stabilizers (for R and B rounds), and (iv) the stabilizers of the check group. We list the topological order of the ISGs in each round of the schedule in Table I. Explicit circuits to map the ISGs to the canonical form of the 3D TC (or two copies of it) are given in the supplementary *Mathematica* file. The counting of logical qubits is described in Appendix B.

We note that the rewinding GBRBGR schedule ensures that, in each round, there is an extensive number of constant-weight evolved condensation terms. This is not the case for the 3-round schedule RGB, which has an ISG that is a stack of 2D TCs with nonlocal stabilizers. Intuitively, rewinding the schedule stops the condensation terms from becoming nonlocal. We also note that the automorphism of logical operators is trivial, which follows from the rewinding property, discussed in Sec. II 2.

### 1. Splitting into two copies of 3D toric code

Interestingly, the B-ISGs and the R-ISGs are FDLQC-equivalent to two copies of the 3D TC, up to nonlocal stabilizers. Here, we elaborate on the mechanism by which the single 3D TC splits into two copies of the 3D TC via measurements. In short, the constant-weight evolved condensation terms can be interpreted as short string operators that create pairs of  $e$  anyons on the next-nearest neighbor octagons of the 2D square-octagon lattices. The configuration of evolved condensation terms is such that the ISG is FDLQC-equivalent to two copies of the 3D

TC with a constraint on the logical subspace given by the condensation terms that evolve into nonlocal stabilizers.

The fact that two copies of 3D TC arise in the B-ISG is best understood in the effective picture of TC layers. In Sec. IV B, we showed that in the B- and R-ISGs, we get TCs on rotated lattices with an effective qubit on each square plaquette of the square-octagon lattice. The B-ISG of the 3D Floquet TC can hence be understood as a coupled layer construction starting from rotated 2D TC layers stacked along three orthogonal directions as shown in Fig. 8.

In the effective description of 2D rotated TC layers, the evolved condensation operators act as 4-qubit Pauli  $X$  operators which create pairs of  $e$ -anyons across intersecting layers, with the violations of  $Z$ -stabilizers in the 2D rotated TCs corresponding to the  $e$ -anyons. The evolved condensation terms are illustrated on the effective lattice using thick red edges in Fig 8(b). The fact that these evolved condensation terms belong to the stabilizer group implies that only certain products of  $Z$ -stabilizers of the 2D layers, as shown in Fig. 8(c), survive as stabilizers after condensation. The violations of these products of  $Z$ -stabilizers correspond to the  $e$ -charges of the two 3D TCs.

Given the structure of the evolved condensation terms, the  $e$ -charges on nearest-neighboring cubes, in fact, belong to inequivalent superselection sectors. Hence, we label them as  $e_1$  and  $e_2$  corresponding to the two copies of the 3D TC. This illustrates that the two 3D TCs “live” on two sublattices of the full cubic lattice.

We now consider the two R-ISGs appearing in the GBRBGR schedule. We label these two consecutive R-ISGs as the  $\text{R}^{(1)}$ -ISG and the  $\text{R}^{(2)}$ -ISG. The key difference in the  $\text{R}^{(1)}$ -ISG, compared to the preceding B-ISG, is that we now have 4-qubit Pauli  $Z_{\text{eff}}$  condensation operators in the effective description of 2D rotated TC layers. The effective 2D rotated TC  $X_{\text{eff}}$  ( $Z_{\text{eff}}$ ) stabilizers are also now changed to  $Z_{\text{eff}}$  ( $X_{\text{eff}}$ ) stabilizers, since the

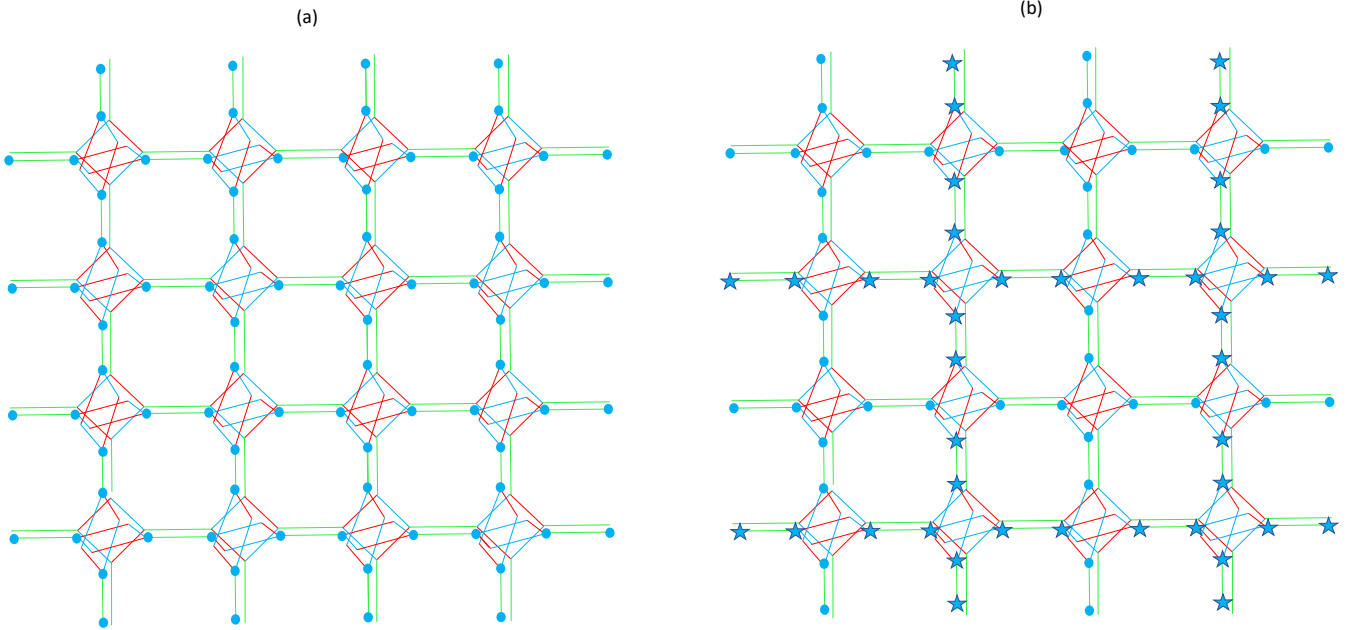
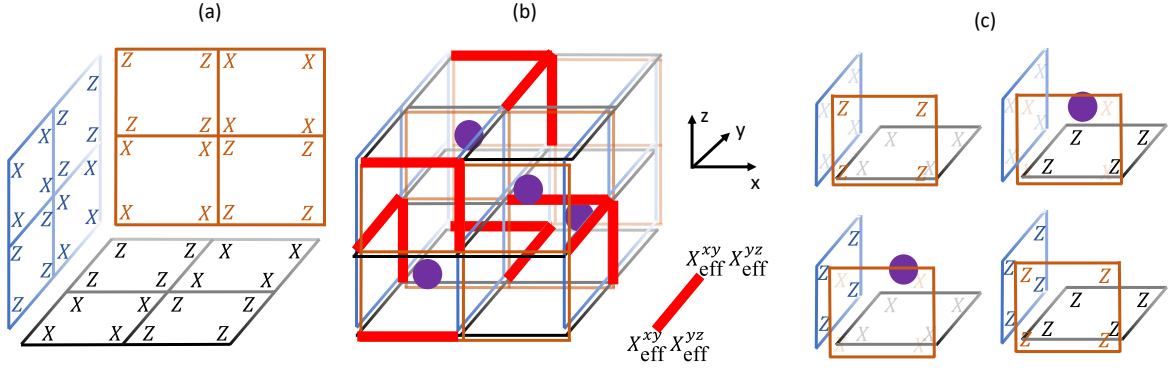


FIG. 9. (a) A logical membrane operator of the 3D TC instantaneous stabilizer group in rounds 1 and 5 (measurement of green checks); the membrane is a product of  $m$ -logical strings (made of Pauli  $Z$  operators shown as blue dots) of the 2D TCs in the planes orthogonal to the membrane. (b) In the B-round, the membrane operator splits into two membranes of  $Z$  operators belonging to two different 3D TCs. One membrane is a product of the blue dots, while the other is a product of the blue stars.

$[[4,1,2]]$  codes on the squares now have  $XX$  checks as stabilizers. Thus, this R-ISC is equivalent to the B-ISC up to a basis change, and we again get two copies of 3D TC (up to nonlocal stabilizers). The full configuration of evolved condensation terms in the unit cell is shown

in Fig. 13(b). The nonlocal stabilizers, in this case, are the same as those of the B-ISC in Fig. 10, but with Pauli  $Y$  operators replaced by Pauli  $X$  operators. These can be obtained by multiplying the nonlocal stabilizers of the B-ISC by the B-checks.

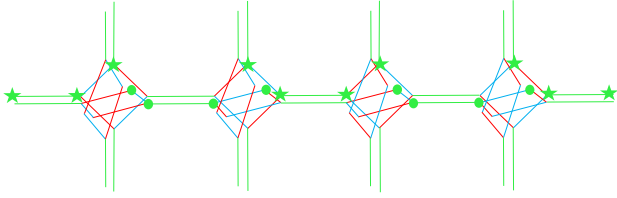


FIG. 10. A nonlocal stabilizer made of Pauli  $Y$  operators (shown with green stars and dots) in the B-ISG. The stars and dots belong to different foliations. Two out of the three two-qubit condensation operators on each octahedron evolve into nonlocal stabilizers along different nontrivial cycles. The nonlocal stabilizer is a product of two  $e$  logical string operators from the G-ISG. These string operators are no longer stabilizer equivalent in B-ISG as they are logical string operators of two different copies of 3D TCs.

In the  $R^{(2)}$ -ISG, the condensation operators are 4-qubit  $X_{\text{eff}}^{\otimes 4}$  and 3-qubit  $X_{\text{eff}}^{\otimes 3}$ ; the microscopic representations are shown in Fig. 7(d) and the effective representations are shown in Fig. 13 along with the configuration of condensation operators in the unit cell. We again get two copies of 3D TCs (up to nonlocal stabilizers) as the ISG. The nonlocal stabilizers, in this case, are similar to those of B-ISG, but shifted.

#### D. Boundary construction

We now consider a boundary construction for the 3D Floquet TC. Since the 3D Floquet TC is based on a coupled layer construction, we start by reviewing the boundaries for the 2D Floquet TC on the square-octagon lattice [3, 4]. We consider in particular the truncation of the square-octagon lattice shown in Fig. 11(a). Here, any check that is truncated is included in the check group as a single-qubit check. In the first R-ISG of the schedule GBRBGR, we get  $m$ -boundaries (i.e., smooth boundaries) where the truncation cuts through the blue and red bonds, and  $e$ -boundaries (i.e., rough boundaries) where the truncation cuts through the green bonds. After half a period of the rewinding schedule, the boundaries switch types.

We now use this construction of boundaries for the 2D code to determine the boundaries of the 3D Floquet TC. The truncation for the three foliations of square-octagon layers is specified in Fig. 11(b). For one of the foliations, the truncation goes through only the blue and red bonds while for the other two, the truncation goes through the red and blue bonds on the top and bottom and green bonds on the left and right sides. The resulting 3D Floquet TC is such that, for each ISG, we have boundaries that condense the point-like anyons on the left and right and the loop-condensing boundaries on the remaining four sides, as in Fig. 11(c).

We note that the particular choice to truncate the blue and red bonds on the lower halves of the square plaquettes ensures that in the 3D Floquet TC lattice, the

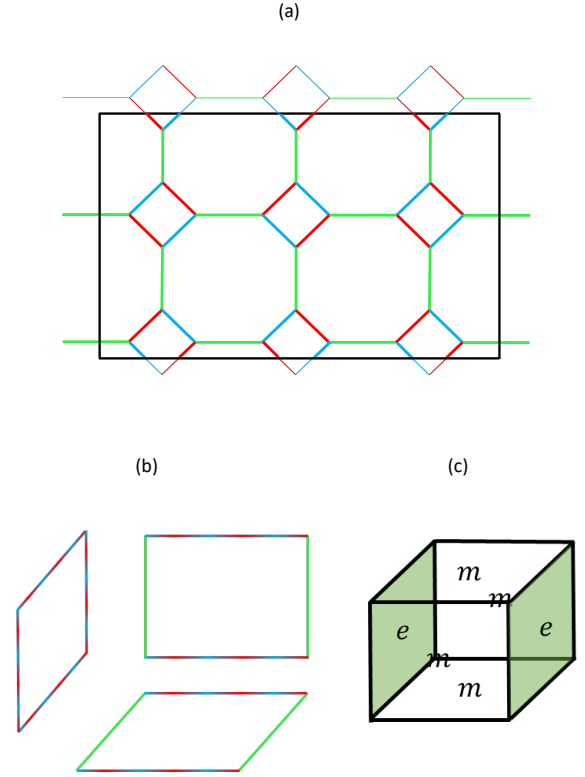


FIG. 11. (a) Truncation of a layer of the square-octagon lattice in the 2D Floquet TC. (b) The boundary truncations for the square-octagon layers that form the lattice for the 3D Floquet TC. (c) Boundaries for a planar configuration of the 3D Floquet TC: we get  $e$ -condensing boundaries on the left and right while the  $m$ -condensing boundaries on the other 4 sides. Note that in the ISGs that are FDLQC-equivalent to two copies of 3D TC, the boundary labeled  $e$  should be interpreted as having two sublattices, one condensing  $e_1$  and one condensing  $e_2$ ; similar for the boundary labeled  $m$ .

two-qubit condensation checks in the G-ISG are never truncated. This choice can nonetheless lead to truncated evolved condensation terms. The truncated condensation terms survive as stabilizers along the boundary with truncated green bonds, while they do not survive along the boundaries with truncated blue and red bonds, since they do not commute with the single-qubit blue and red checks.

The result of these truncations is that, for each ISG, the charges (possibly two types  $e_1$  and  $e_2$ , depending on the round) are condensed on the right and left boundaries, while the loop-like excitations are condensed on the remaining four sides.

It is straightforward to understand this result from the perspective of the 2D TCs on the effective lattice. In the G-ISG, the  $e$ -charge is associated with the product of octagonal plaquettes, which also correspond to  $e$ -anyons of the layers. Since the truncation through green checks creates an  $e$ -condensing boundary for the 2D G-ISGs, the  $e$ -charge of the 3D code also condenses at that boundary. Similarly, the loop excitations are condensed at the

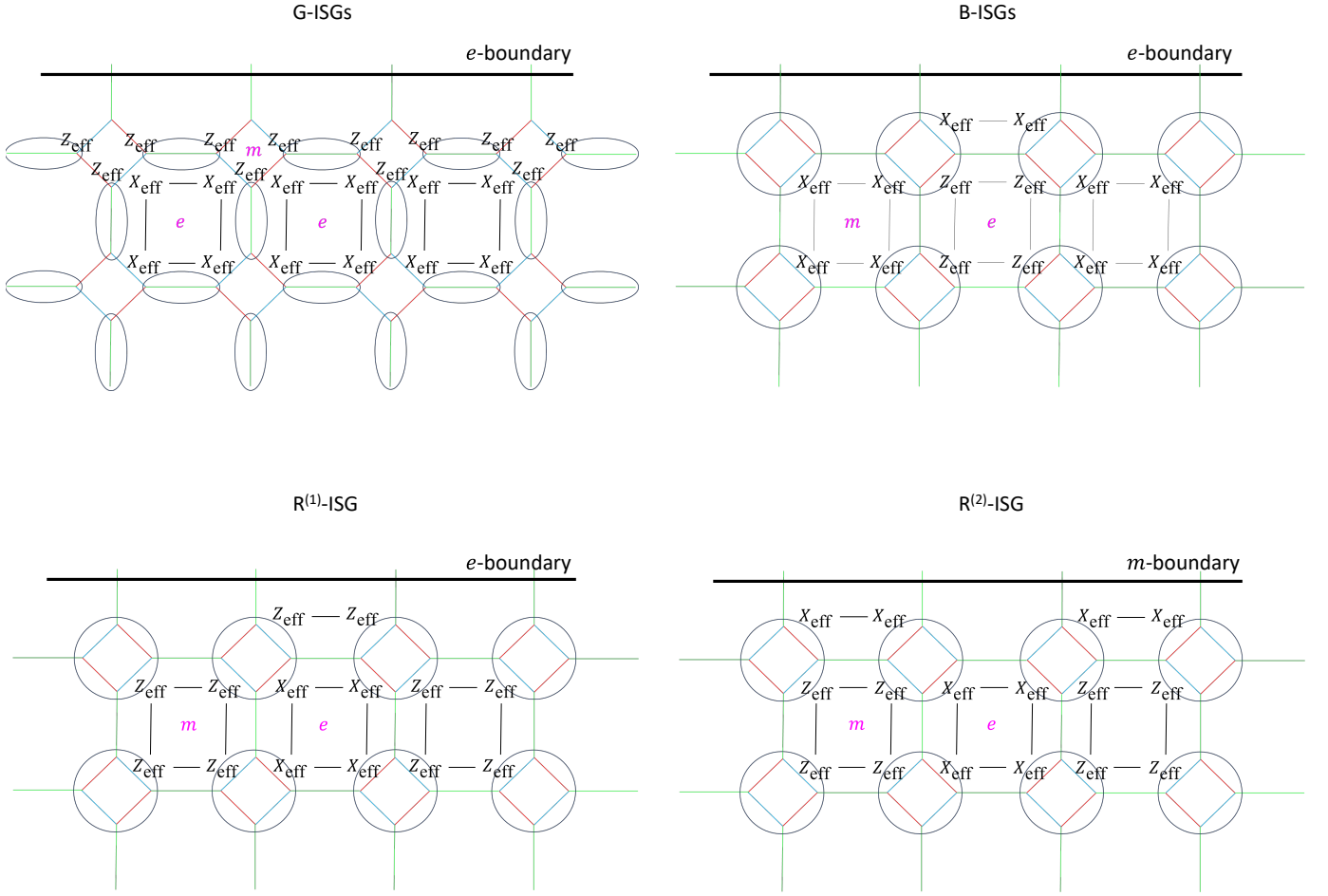


FIG. 12. Truncation through the green checks in the ISGs in the 2D Floquet TC on the square octagon lattice with the GBRBGR schedule. For the G-ISGs, the effective qubits (illustrated using ellipses) live on the green edges, and for the B- and R-ISGs, the effective qubits (illustrated using circles) live on the square plaquettes. The bulk and boundary stabilizers are written in terms of the effective Pauli operators. Top: the truncation through green checks condenses the  $e$ -anyons (convention chosen is shown) in the G- and B-ISGs. Bottom: The truncation through green checks in the two R-ISGs. For these two R-ISGs, the boundary undergoes an automorphism in its type due to the bulk automorphism.  $R^{(1)}$ -ISG indicates the ISG in the first R-round and  $R^{(2)}$ -ISG indicates the ISG in the second R-round in the sequence. The truncation through green checks describes an  $e$  ( $m$ ) boundary in the  $R^{(1)}$ -ISG ( $R^{(2)}$ -ISG) respectively for the convention chosen.

truncation through the blue and red bonds.

In both of the B-ISGs, we have the effective picture of the 2D rotated TCs, and the bulk condensation operators are of the form  $X_{\text{eff}}^{\otimes 4}$ , which implies that the  $e$ -charges are associated with products of  $Z_{\text{eff}}$ -stabilizers. For the B-ISG of the 2D Floquet code, the truncation through green checks condenses the violations of the  $Z_{\text{eff}}$ -stabilizers supported on the octagonal plaquettes consisting of red and green edges. This is illustrated in Fig. 12(c). Thus, for the B-ISG of the 3D Floquet code, at the truncation through green bonds, we condense the violations of these  $Z_{\text{eff}}$ -stabilizers, corresponding to point-like excitations, and at the truncation through blue and red bonds, we condense the violations of the  $X_{\text{eff}}$ -stabilizers corresponding to loop-like excitations.

After the B-round, we have the  $R^{(1)}$ -ISG. For both of the R-ISGs, we can again use the effective picture of rotated toric layers along three foliations and the action

of evolved condensation terms. For the 2D rotated TC layers, the truncation through green bonds gives an  $e$ -( $m$ -) boundary in the  $R^{(1)}$ -ISG ( $R^{(2)}$ -ISG). This is illustrated in Fig. 12, where the stabilizers at the boundary are shown in terms of the effective Pauli operators. The condensation operators in the  $R^{(1)}$ -ISG and  $R^{(2)}$ -ISG are given by  $Z_{\text{eff}}^{\otimes 4}$  and  $X_{\text{eff}}^{\otimes 4}$ , respectively, and are shown in Fig. 13. In the  $R^{(1)}$ -ISG, since the condensation operators are given by  $Z_{\text{eff}}^{\otimes 4}$ , the stabilizer products corresponding to  $e$ -charges ( $m$ -loops) are given by the  $X_{\text{eff}}$  ( $Z_{\text{eff}}$ ) stabilizers. Hence, the truncation through green bonds condenses the loop-like excitations. Similarly, in the  $R^{(2)}$ -ISG, the condensation operators are given by  $X_{\text{eff}}^{\otimes 4}$  and  $X_{\text{eff}}^{\otimes 3}$  as shown in Fig. 13 and the stabilizer products corresponding to  $e$ -charges ( $m$ -loops) are given by the  $Z_{\text{eff}}$  ( $X_{\text{eff}}$ ) stabilizers. The truncation through green bonds again condenses the loop-like excitations. Similarly, the



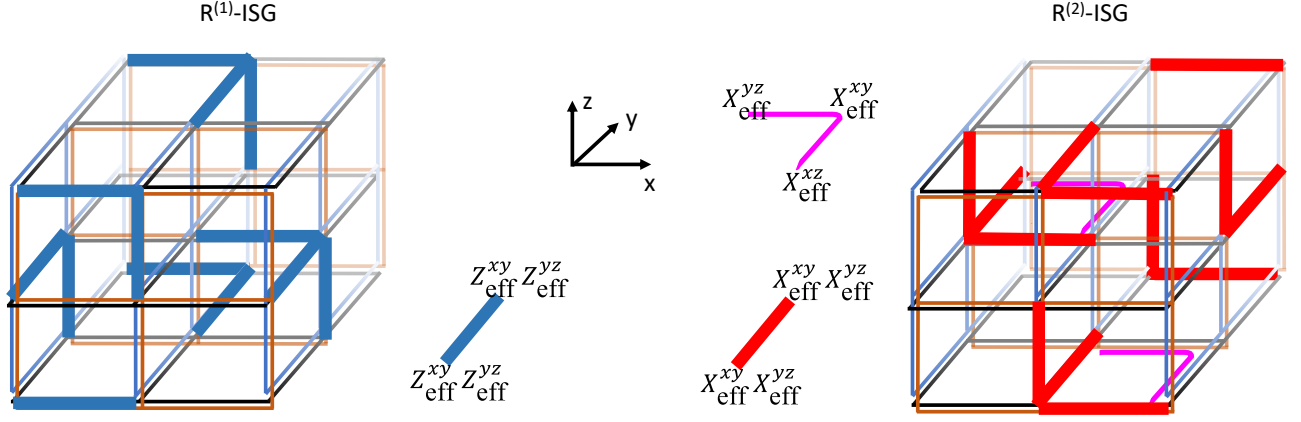


FIG. 13. Configuration of condensation operators in the two R-ISGs is shown in the 3-foliated stack of rotated lattice TC layers (the effective description of the square-octagon layers in the R-round). In the  $R^{(1)}$ -ISG ( $R^{(2)}$ -ISG), the condensation operators are  $Z_{\text{eff}}^{\otimes 4}$  ( $X_{\text{eff}}^{\otimes 4}$  in red and  $X_{\text{eff}}^{\otimes 3}$  in pink) operators; representation for 4-qubit condensation operators along the  $y$ -direction and for the 3-qubit condensation operator are shown; here  $xy$  and  $yz$  in Pauli operators  $X_{\text{eff}}^{xy}$  and  $X_{\text{eff}}^{yz}$ , denote the foliations the qubits belong to. The microscopic representation of the 3-qubit condensation operator  $X_{\text{eff}}^{\otimes 3}$  on the 3D Floquet code lattice is shown below the effective representation. Thus, the  $e$ -charges of the 3D TCs correspond to products of  $X_{\text{eff}}$  ( $Z_{\text{eff}}$ ) stabilizers in the  $R^{(1)}$ -ISG ( $R^{(2)}$ -ISG) and the  $m$ -loops have  $Z_{\text{eff}}$  ( $X_{\text{eff}}$ ) stabilizers in the  $R^{(1)}$ -ISG ( $R^{(2)}$ -ISG). The truncation through the green checks, hence, corresponds to the charge-condensing boundaries.

truncation through the blue and green bonds, as shown in Fig. 11(a), always condenses the point-like charges of the 3D TCs. To conclude, even though the 2D Floquet code layers undergo a boundary transformation from  $e$ -type to  $m$ -type, the 3D Floquet TC boundaries condense the same type of excitations in each ISG.

### E. Transversal non-Clifford gate

One key computational advantage of the 3D TC is that it allows for an implementation of the transversal logical non-Clifford gate [13, 21]. Such an advantage is retained for our 3D Floquet TC. This is because the 3D TC in the G-ISG has the conventional cubic lattice form (up to concatenation with 2-qubit repetition codes). We can stack the 3D Floquet TC with two copies of the 3D TC on the checkerboard lattice to yield the transversal  $CCZ$  gate as an on-site symmetry of the stabilizer group [13, 21]. More specifically, on a system with both the 3D Floquet TC and two 3D checkerboard lattice TCs, we can perform the transversal logical  $CCZ$  gate in the round of the Floquet cycle in the G-ISG. Since the logical information is preserved under subsequent measurements for both the 3D Floquet TC and the 3D checkerboard lattice TCs, one can wait to do the  $CCZ$  gate transversally in the G-ISG and then proceed with subsequent rounds.

The checkerboard lattice surface code (planar variant) can be obtained as instantaneous stabilizer codes of the 3D subsystem TC, which uses measurements of three-qubit checks. [12]. Hence, one can stack the planar variant of our 3D Floquet code with two copies of the 3D subsystem TC to do the non-Clifford  $CCZ$  gate in the G-round of the 3D Floquet TC.

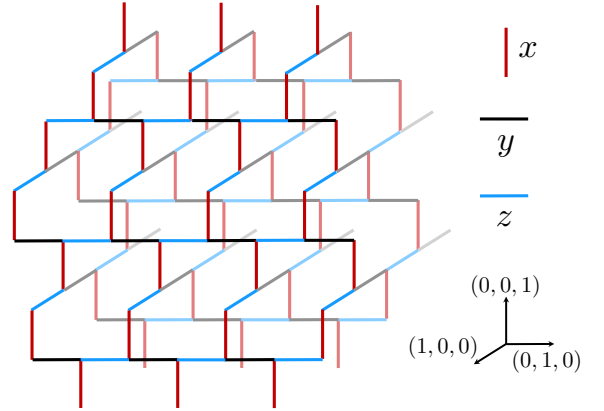


FIG. 14. The 3D fTC is defined on a trivalent lattice. The edges are labeled by  $x$  (red),  $y$  (black), and  $z$  (blue).

## V. 3D FLOQUET FERMIONIC TORIC CODE

In this section, we present a Floquet code that has ISGs that are FDLQC-equivalent to the 3D fermionic TC (fTC) [14, 27]. This construction is based on the 3D generalization of Kitaev's honeycomb model introduced in Ref. [15]. For this example, each ISG is FDLQC-equivalent to the 3D fTC. This Floquet code, however, only encodes a single logical qubit on a system with periodic boundary conditions, due to inadvertently measuring a subset of the logical operators. We make use of a rewinding schedule to avoid measuring the logical operators for the remaining logical qubit.

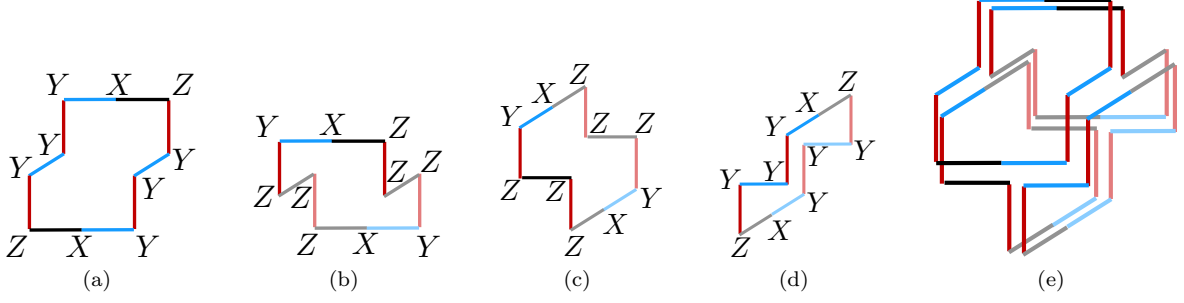


FIG. 15. There are four types of local generators of the stabilizer group: the (a) front, (b) back, (c) right, and (d) left armchair stabilizers, which are equivalent to a product of checks around the plaquette. (e) The four armchair stabilizers satisfy a local relation.

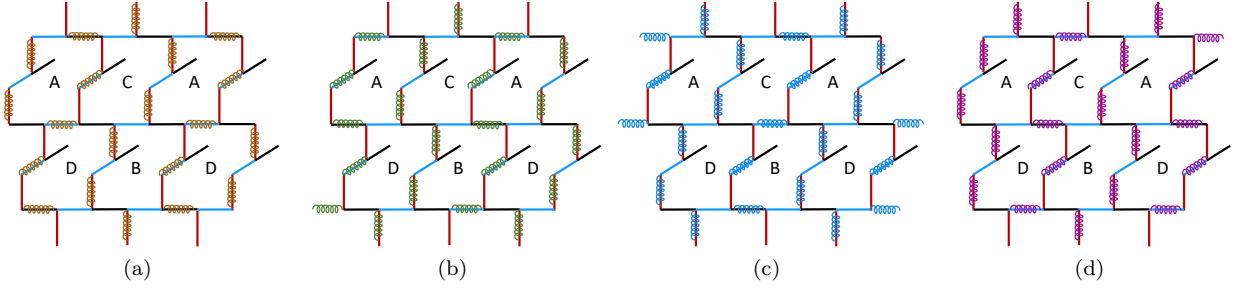


FIG. 16. (a)-(d) The front-facing armchair stabilizers can be inferred from five rounds of measurements. The measurements in rounds 0-3 are shown in brown, green, blue and pink, respectively. The final round is a repetition of round 0. The measurements for the back-facing and left-facing armchairs are defined in a similar way.

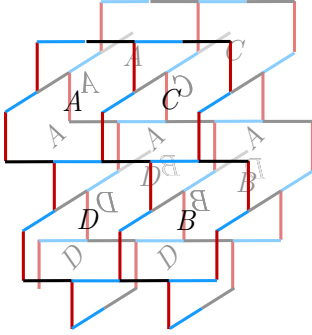


FIG. 17. There are 4 labels: A, B, C, and D, for the armchairs. The labels for front-facing armchairs are written with the usual orientation of A, B, C, D, while those for the right- and back-facing armchairs are tilted and reflected. The labels for the B and C right-facing armchairs do not appear in this portion of the lattice.

#### A. 16-round measurement schedule

Our first example is defined on the trivalent lattice in Fig. 14 with periodic boundary conditions.<sup>6</sup> We place a

qubit at each vertex and label the edges with  $x$ ,  $y$ , and  $z$ , as in Fig. 14. The 2-body check operators on the edges  $x$ ,  $y$ , and  $z$  are  $XX$ ,  $YY$ , and  $ZZ$ , respectively.

Similar to the 2D Floquet TC in Section IV B, the stabilizers of the check group are generated by products of the 2-body checks along closed paths, which includes stabilizers supported on non-contractible paths. The local generators of the stabilizer group are 10-body products of check operators around a plaquette. Given the shape of these plaquettes, we refer to these stabilizers as the ‘armchair’ stabilizers. There are four possible orientations for the armchairs: front-, back-, left-, or right-facing [see Fig. 15(a)-(d)]. For each 3-cell, there exists a local relation between four armchair stabilizers, with one facing in each direction as pictured in Fig. 15(e). Thus, we only need to infer the measurement outcomes of three out of the four orientations of armchair stabilizers.

Our measurement schedule is designed to extract the syndrome for one orientation of armchair stabilizers at a time. We use a separate set of five rounds of measurements to infer the front-, back-, and right-facing armchair

<sup>6</sup> We note that any 2D lattice can be coarse-grained into a square lattice with a constant number of vertices per unit cell. Since

the square lattice is 4-valent, the model can be defined on a 3D diamond lattice by replacing the sites of the diamond lattice with the unit cell of the square lattice model. The lattice in Fig. 14 can be constructed in this way starting from the honeycomb lattice.

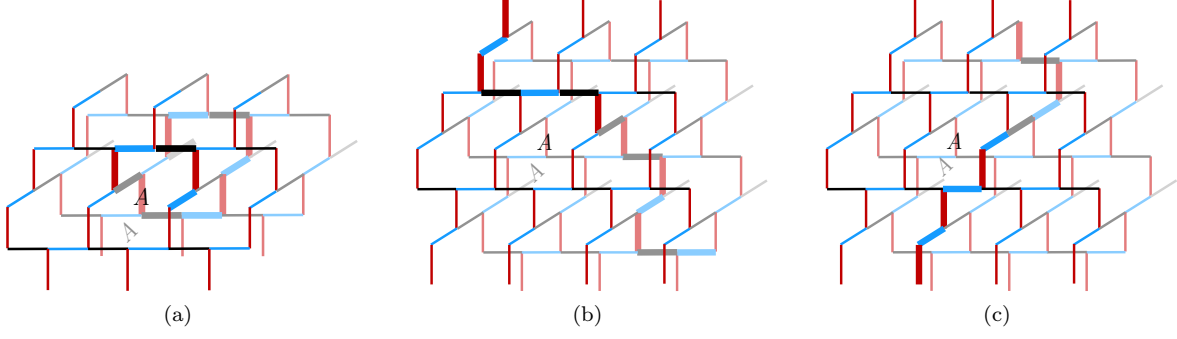


FIG. 18. Logical operators are inadvertently measured using the FBR schedule, when transitioning between inferring the armchair stabilizers with different orientations. The logical operators measured in the transitions (a) F to B, (b) B to R, (c) R to F are shown. We note that the two specified  $A$  plaquettes is sufficient to determine the labeling of the other plaquettes.

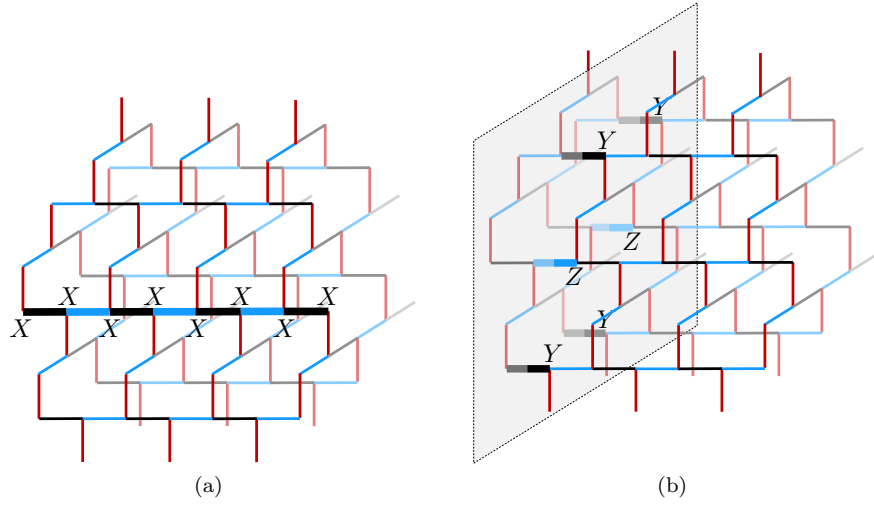


FIG. 19. The Floquet 3D FTC encodes one logical qubit. (a) The  $Z$  logical operator is a product of 2-body check operators along the  $(0, 1, 0)$  direction. (b) The  $X$  logical operator can be represented by an operator supported on a membrane that is orthogonal to the string of the logical  $Z$  operator.

stabilizers. We do not need to infer the measurement of the left-facing armchairs, given the local relation in Fig. 15(e). The five rounds of measurements are shown in Fig. 16 and are labeled as 0, 1, 2, 3, and 0, where the 0 round is repeated at the end of the cycle. If we label the armchairs of a unit cell as  $A$ ,  $B$ ,  $C$ , and  $D$ , as in Fig. 17, we see that after applying consecutive 01, 12, 23, and 30 checks, the  $A$ ,  $B$ ,  $C$ , and  $D$  armchair stabilizers are inferred, respectively. Therefore, the above schedule measures all the armchair stabilizers for an orientation, as desired. We proceed similarly for the back- and right-facing armchair stabilizers.

Naively, a potential measurement schedule is to periodically measure the sequence FBR, where F, B, and R stand for the 5-round measurement schedules for extracting the front-, back-, and right-facing armchair syndromes. This schedule, however, does not exhibit any dynamically generated logical qubits. This is because, in transitioning between the orientations, e.g., F to B, we inadvertently measure the stabilizers supported along

non-contractible paths around the torus. Specifically, in transitioning from F to B, B to R, and R to F, we measure the logical operators supported on non-contractible paths along the  $(1, 0, 0)$ -,  $(0, 1, 1)$ -, and  $(1, 0, 1)$ -directions, respectively (see Fig. 18). As such, the FBR schedule gives a Floquet code that does not encode any qubits.

To rectify this, we rewind the schedule at the level of the armchair orientations, i.e., we periodically measure the sequence FBFR. This sequence avoids the transition from B to R, implying that we do not inadvertently measure the stabilizer supported on a non-contractible path along the  $(0, 1, 1)$ -direction. We note that the second 5-round sequence F can be replaced with a single round of 0 measurements for the front-facing armchair. In summary, our schedule consists of repeating the following sequence of 16 rounds of measurements:

$$(0, 1, 2, 3, 0)_F(0, 1, 2, 3, 0)_B(0, 1, 2, 3, 0)_R, \quad (5)$$

where the subscripts denote the orientations of the armchairs. This modification to the FBR schedule ensures

that we retain a single dynamically generated logical qubit.

After each round of measurements, the ISG is FDLQC-equivalent to the 3D fTC. To verify this, we use ERG to construct an explicit circuit to map the ISGs to the canonical form of the 3D fTC, as shown in the supplementary *Mathematica* file. We note that, at a high level, the stabilizers of the check group generate a so-called anomalous 2-form symmetry [27], i.e., the symmetry operators (the stabilizers) are supported on loops and the point-like excitation at the endpoint of a truncated string operator have nontrivial (in this case fermionic) exchange statistics. This implies that each ISG has an anomalous 2-form symmetry, which is sufficient to guarantee that the ISGs necessarily have an emergent fermion.

The 3D fTC has three logical qubits on a system with periodic boundary conditions. However, given that our schedule inadvertently infers the measurement of the stabilizers supported on non-contractible paths along the  $(1, 0, 0)$ - and  $(1, 0, 1)$ -directions, our Floquet 3D fTC encodes a single logical qubit. The logical Pauli  $Z$  operator can be represented by a product of 2-body check operators along the  $(0, 1, 0)$ -direction, as in Fig. 19(a). This can be interpreted as the nonlocal stabilizer of the check group that remains unmeasured throughout the measurement schedule. The logical Pauli  $X$  operator can be represented by an operator supported on a membrane perpendicular to the  $(0, 1, 0)$ -direction [Fig. 19(b)]. We find that the sequence  $(0, 1, 2, 3, 0)_F$  implements the trivial automorphism (and similarly for the B and R sequences). Thus, due to the rewinding nature of the FBFR schedule, the full 16-round period undergoes a trivial automorphism.

## VI. DISCUSSION

In this paper, we constructed examples of topological Floquet codes with ISGs that are FDLQC-equivalent to the 2D color code, the 3D TC, and the 3D fermionic TC. To construct the 3D Floquet codes, we used the idea of rewinding the measurement schedule. Below, we comment on some aspects of our Floquet codes and discuss directions for future work.

### 1. Local reversibility and possible fault-tolerance

In Ref. [16], it was suggested that the local reversibility of a topological Floquet code could imply the existence of a non-zero threshold. We show below that our schedules for the 2D Floquet color code are locally reversible and we expect the same to hold for our 3D Floquet codes. We first state the definitions: An ISG is locally generated *above* a subgroup if there is a set of local operators that along with the subgroup elements form a generating set of the ISG. The ISGs in our Floquet codes are all locally generated above a subgroup, with the subgroup being

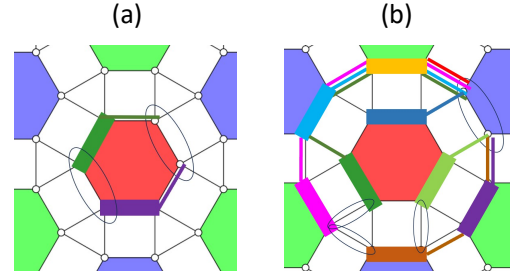


FIG. 20. (a) Local reversibility of ISGs in rounds 0 and 1 of Floquet color code. The 0-checks on the red hexagon are marked using thick edges. Their conjugate partner 1-checks are marked using a thin edge of the same color as the 0-check. The circled checks are the checks that we do not need to consider to form the pairs of conjugate local operators *above* the intersection of 0-ISG and 1-ISG; the intersection includes the product of 0-checks and the product of 1-checks around the hexagon. (b) Local reversibility of ISGs in rounds 1 and 2 of Floquet color code. The 1-checks on the red hexagon are marked using thick edges. Their conjugate partners are products of 2-checks that are marked using thin edges of the same color as the 1-check. We do not need to consider the circled checks in the pairs of conjugate local operators *above* the intersection of 1-ISG and 2-ISG; the intersection contains the product of all 1-checks on the red inflated hexagon and the inflated hexagon stabilizers of the check group.

the intersection of two ISGs. Now, two ISGs, let's say 0-ISG and 1-ISG, form a locally reversible pair if there is a choice of local generating sets above the intersection  $0\text{-ISG} \cap 1\text{-ISG}$ , 0-LGI and 1-LGI respectively such that one generator from 0-LGI (1-LGI) anticommutes with exactly one generator from 1-LGI (0-LGI). Such anticommuting pairs are referred to as conjugate pairs.

In the Floquet color code, the intersection  $0\text{-ISG} \cap 1\text{-ISG}$  contains the product of 0-checks and the product of 1-checks around each hexagon. Hence, we can remove one 0-check and 1-check from our local generating sets. The removed checks and conjugate pairs for 0- and 1-ISGs are illustrated in Fig. 20(a). The pairs of ISGs in rounds 1 and 2 as well as rounds 2 and 0 are also locally reversible. We now explain this for pair of rounds 1 and 2. The intersection  $1\text{-ISG} \cap 2\text{-ISG}$  includes the product of 1-checks on the inner and outer boundary of the red-inflated hexagons and the stabilizers of the check group on each of the three inflated hexagons. Hence we remove one 1-check and three 2-checks on the red-inflated hexagon from our consideration because we need to form the conjugate pairs only above the intersection. Then, the conjugate pairs are the products of 2-checks in a chain whose one end intersects with its conjugate partner 1-check in one qubit and the other end intersects the removed 1-check. The removed checks and conjugate pairs for 1- and 2-ISGs are illustrated in Fig. 20(b).

We expect that the schedules for the 3D Floquet TC and 3D Floquet fTC are also locally reversible. There are non-local stabilizers in the ISGs but they exist as stabilizers in the intersection of any consecutive pair of ISGs



and do not preclude the existence of locally conjugate generating sets. Here, we discuss only the reversibility of ISGs in the 3D Floquet TC. We can consider the pair of ISGs, 3D TC in the G-round, and a subspace of two copies of 3D TCs in the B-round. Any string logical operator of G-ISG 3D TC is indeed also a logical string operator of the ISG of two copies of 3D TCs up to nonlocal stabilizers. Hence, the two ISGs share their full set of logical operators and hence, as defined in Ref. [16], this is a sufficient criterion for reversibility.

## 2. 3D Floquet toric code on a fractal

In Sec. IV D, we discussed the planar realization of the 3D Floquet TC. It is known that in the 3D TC, one can punch holes with smooth boundaries to build a fractal lattice code embedded in 3D with fractal Hausdorff dimension  $2 < D_H < 3$  [31, 32]. Starting with the G-ISG, we can, in principle, punch holes with smooth boundaries by truncating the checks across the red and blue bonds. In subsequent rounds, as discussed in Sec. IV D, these boundaries always remain loop-condensing boundaries, although they may become loop-condensing boundaries of two copies of the 3D surface code. Thus, we expect our construction with holes to yield a Floquet code with ISGs that are fractal surface codes embedded in 3D [31, 32]. It would be interesting to further explore such Floquet codes on fractal lattices for both memory and computation.

## 3. Bifurcation of topological order under measurements

In the 3D Floquet TC, we observed that as the condensation operators evolved into 4-qubit operators, we obtained the ISG of two copies of the 3D TC, up to nonlocal stabilizers. Starting from stacks of TC, if we are allowed measurement of higher-but-constant weight condensation operators, we can obtain a higher constant number of copies of 3D TC. It would be interesting to see if there is a Floquet code arising from coupled layers, such that the condensation operators always evolve by a *constant* factor so that topological order bifurcates under every round of measurements. Such a bifurcation is known to occur for fracton topological order under entanglement renormalization group [28–30]. However, topological orders are conventional fixed points under the entanglement renormalization group. Thus, it is curious if, under specialized measurement sequences, conventional topological order can exhibit bifurcation. On the other hand, it would be also interesting if there is a fundamental obstruction to having such measurement dynamics.

## 4. Classification of measurement schedules

One fundamental question that arose in this work is what schedules exist for a given check group and what automorphisms of the logical information are exhibited by them. For instance, we wrote three schedules for the Floquet color code, one which exhibited a  $\mathbb{Z}_3$  automorphism of logical operators, a rewound version that exhibited a trivial automorphism and another 6-round schedule that exhibits a trivial automorphism. It would be interesting whether there is a notion of equivalence between the two schedules with a trivial automorphism, such as the notion of simple equivalence discussed in Ref. [16]. It would also be interesting to have a recipe to construct the inequivalent Floquet codes, given a set of checks on a lattice. For the 3D Floquet fTC, we presented a schedule with 16 rounds that preserved one logical qubit. There could exist a more efficient schedule and also one that preserves all logical qubits. However, our attempts with different schedules and on different trivalent lattices were unsuccessful. Hence, we leave this as a future direction.

One potential source of inspiration for new schedules, although, not periodic, come from Refs. [33] and [34], which considered weighted random measurements of  $XX$ ,  $YY$ , and  $ZZ$  checks in the honeycomb Floquet code. In particular, they found a regime in which the topological information is protected. One could consider such schedules for our Floquet code examples, especially, for the 3D Floquet fTC. We were not able to preserve all three logical qubits, but this may be possible with an appropriate random measurement schedule. Similar to the 2D case, we expect that there is a regime in which all three logical qubits are preserved under the dynamics.

## 5. Condensation picture

Following Ref. [7], it may be insightful to understand the Floquet codes in this work in terms of sequences of condensations in a parent stabilizer code. In general, it may be challenging to identify a suitable parent stabilizer code, but for our examples, the stabilizer group of the check group is nontrivial. This means that a natural generating set for the stabilizer group of the parent stabilizer group is the stabilizers of the check group and a maximal set of local Pauli operators that commute with them. The measurements of the check operators can then be interpreted as condensing an excitation of this parent stabilizer code, resulting in the ISGs of the Floquet code. This code is FDLQC-equivalent to two copies of color code or four copies of TC. The exact circuit to map this code to four copies of the TC is given in the supplementary *Mathematica* files. The complete pictures of condensation in this parent code for our three variants of the Floquet color code still needs investigation. For the 3D Floquet TC, a natural choice of parent stabilizer code is a stack of color codes, since the color code is a parent stabilizer code for the 2D Floquet TC [35]. For

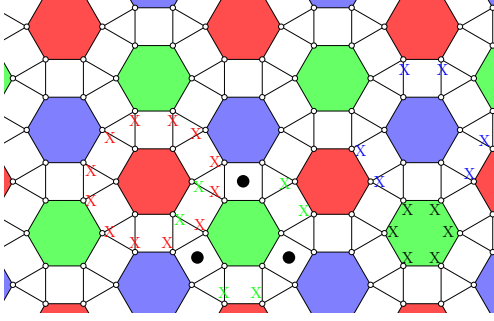


FIG. 21. Parent stabilizer code for the Floquet color code. This stabilizer code contains the stabilizers of the check group and is FDLQC-equivalent to two copies of the color code. The stabilizer generators include products of  $X$  or  $Z$  Pauli operators on the inner and outer boundaries of the inflated hexagons, as shown. For two colors of the inflated hexagon (blue and green inflated hexagons in the figure) the stabilizers on the exterior boundary are six-qubit operators while for the third (red inflated hexagon in the figure), they are twelve-qubit operators – the  $X$ -stabilizer on the exterior boundary of the red inflated hexagon is shown. The other stabilizers are  $X$  and  $Z$  stabilizers on the squares that lie between the green and blue hexagons – these stabilizers are marked by black dots in the figure.

the Floquet color code, we write down a parent stabilizer code, as shown in Fig. 21.

## ACKNOWLEDGEMENT

We thank the authors of Ref. [36] and Ref. [37] for informing us about their work on Floquet color codes. N.T., J.S., and T.D.E. acknowledge the 2023 Boulder Summer School on Non-Equilibrium Quantum Dynamics, where part of this work was completed. A.D. is supported by the Simons Foundation through the collaboration on Ultra-Quantum Matter (651438, AD) and the Institute for Quantum Information and Matter, an NSF Physics Frontiers Center (PHY-1733907). N.T. is supported by the Walter Burke Institute for Theoretical Physics at Caltech. J.S. is supported by DOE DESC0022102. The *Mathematica* codes used in this paper are available on GitHub at <https://github.com/dua-arpit/floquetcodes>.

\* [adua@caltech.edu](mailto:adua@caltech.edu)

† [tyler.ellison@yale.edu](mailto:tyler.ellison@yale.edu)

- [1] M. B. Hastings and J. Haah, Dynamically generated logical qubits, *Quantum* **5**, 564 (2021).
- [2] C. Gidney, M. Newman, A. Fowler, and M. Broughton, A Fault-Tolerant Honeycomb Memory, *Quantum* **5**, 605 (2021).
- [3] C. Gidney, M. Newman, and M. McEwen, Benchmarking the Planar Honeycomb Code, *Quantum* **6**, 813 (2022).
- [4] A. Paetznick, C. Knapp, N. Delfosse, B. Bauer, J. Haah, M. B. Hastings, and M. P. da Silva, Performance of planar floquet codes with majorana-based qubits, *PRX Quantum* **4**, 010310 (2023).
- [5] J. Haah and M. B. Hastings, Boundaries for the Honeycomb Code, *Quantum* **6**, 693 (2022).
- [6] M. Davydova, N. Tantivasadakarn, and S. Balasubramanian, *Floquet codes without parent subsystem codes* (2022).
- [7] M. S. Kesselring, J. C. M. de la Fuente, F. Thomsen, J. Eisert, S. D. Bartlett, and B. J. Brown, Anyon condensation and the color code (2022), [arXiv:2212.00042](https://arxiv.org/abs/2212.00042) [quant-ph].
- [8] H. Bombin, D. Litinski, N. Nickerson, F. Pastawski, and S. Roberts, Unifying flavors of fault tolerance with the zx calculus (2023), [arXiv:2303.08829](https://arxiv.org/abs/2303.08829) [quant-ph].
- [9] H. Ma, E. Lake, X. Chen, and M. Hermele, Fracton topological order via coupled layers, *Physical Review B* **95**, 10.1103/physrevb.95.245126 (2017).
- [10] Z. Zhang, D. Aasen, and S. Vijay, The x-cube floquet code, (2022), [arXiv:2211.05784](https://arxiv.org/abs/2211.05784).
- [11] A. Bauer, Topological error correcting processes from fixed-point path integrals (2023), [arXiv:2303.16405](https://arxiv.org/abs/2303.16405) [quant-ph].
- [12] A. Kubica and M. Vasmer, Single-shot quantum error correction with the three-dimensional subsystem toric code, *Nature Communications* **13**, 6272 (2022).
- [13] M. Vasmer and D. E. Browne, Three-dimensional surface codes: Transversal gates and fault-tolerant architectures, *Phys. Rev. A* **100**, 012312 (2019).
- [14] M. Levin and X.-G. Wen, Fermions, strings, and gauge fields in lattice spin models, *Phys. Rev. B* **67**, 245316 (2003).
- [15] S. Mandal and N. Surendran, Exactly solvable kitaev model in three dimensions, *Phys. Rev. B* **79**, 024426 (2009).
- [16] D. Aasen, J. Haah, Z. Li, and R. S. K. Mong, Measurement quantum cellular automata and anomalies in floquet codes, (2023), [arXiv:2304.01277](https://arxiv.org/abs/2304.01277) [quant-ph].
- [17] J. Sullivan, R. Wen, and A. C. Potter, Floquet codes and phases in twist-defect networks (2023), [arXiv:2303.17664](https://arxiv.org/abs/2303.17664) [quant-ph].
- [18] H. Bombin, Topological subsystem codes, *Phys. Rev. A* **81**, 032301 (2010).
- [19] P. Sarvepalli and K. R. Brown, Topological subsystem codes from graphs and hypergraphs, *Phys. Rev. A* **86**, 042336 (2012).
- [20] B. Yoshida, Topological color code and symmetry-protected topological phases, *Phys. Rev. B* **91**, 245131 (2015).
- [21] A. Kubica and M. E. Beverland, Universal transversal gates with color codes: A simplified approach, *Phys. Rev. A* **91**, 032330 (2015).

- [22] H. Bombin, Gauge color codes: Optimal transversal gates and gauge fixing in topological stabilizer codes (2015), [arXiv:1311.0879 \[quant-ph\]](#).
- [23] H. Bombin, M. Kargarian, and M. A. Martin-Delgado, Interacting anyonic fermions in a two-body color code model, *Physical Review B* **80**, [10.1103/physrevb.80.075111](#) (2009).
- [24] H. Bombin, G. Duclos-Cianci, and D. Poulin, Universal topological phase of two-dimensional stabilizer codes, *New Journal of Physics* **14**, 73048 (2012).
- [25] H. Bombin, Structure of 2D Topological Stabilizer Codes, *Communications in Mathematical Physics* **327**, 387 (2014).
- [26] T. D. Ellison, Y.-A. Chen, A. Dua, W. Shirley, N. Tantivasadakarn, and D. J. Williamson, [Pauli topological subsystem codes from abelian anyon theories](#) (2022), [2211.03798](#).
- [27] Y.-A. Chen and A. Kapustin, Bosonization in three spatial dimensions and a 2-form gauge theory, *Phys. Rev. B* **100**, 245127 (2019).
- [28] J. Haah, Bifurcation in entanglement renormalization group flow of a gapped spin model, *Phys. Rev. B* **89**, 075119 (2014).
- [29] W. Shirley, K. Slagle, and X. Chen, Foliated fracton order from gauging subsystem symmetries, *SciPost Phys.* **6**, 041 (2019).
- [30] A. Dua, P. Sarkar, D. J. Williamson, and M. Cheng, Bifurcating entanglement-renormalization group flows of fracton stabilizer models, *Phys. Rev. Res.* **2**, 033021 (2020).
- [31] G. Zhu, T. Jochym-O'Connor, and A. Dua, Topological order, quantum codes, and quantum computation on fractal geometries, *PRX Quantum* **3**, 030338 (2022).
- [32] A. Dua, T. Jochym-O'Connor, and G. Zhu, Quantum error correction with fractal topological codes (2022), [arXiv:2201.03568 \[quant-ph\]](#).
- [33] A. Sriram, T. Rakovszky, V. Khemani, and M. Ippoliti, Topology, criticality, and dynamically generated qubits in a stochastic measurement-only kitaev model (2022), [arXiv:2207.07096 \[quant-ph\]](#).
- [34] A. Lavasani, Z.-X. Luo, and S. Vijay, Monitored quantum dynamics and the kitaev spin liquid (2022), [arXiv:2207.02877 \[cond-mat.str-el\]](#).
- [35] M. S. Kesselring, J. C. M. de la Fuente, F. Thomsen, J. Eisert, S. D. Bartlett, and B. J. Brown, Anyon condensation and the color code (2022), [arXiv:2212.00042 \[quant-ph\]](#).
- [36] M. Davydova, N. Tantivasadakarn, S. Balasubramanian, and D. Aasen, Quantum computation from dynamic automorphism codes (2023), [arXiv:2307.10353 \[quant-ph\]](#).
- [37] A. Townsend-Teague, J. M. de la Fuente, and M. Kesselring, Floquetifying the colour code (2023), [arXiv:2307.11136 \[quant-ph\]](#).
- [38] J. Haah, Lattice quantum codes and exotic topological phases of matter (2013), [arXiv:1305.6973 \[quant-ph\]](#).
- [39] See Supplementary Mathematica files here: <https://github.com/dua-arpit/floquetcodes>.

## Appendix A: Rewinding X-cube Floquet code

The X-cube Floquet code of Ref. [10] has ISGs that are for some rounds, stacks of TC and for other rounds, FDLQC-equivalent to the X-cube model or another fracton model. We propose a rewinding schedule for the X-cube model such that each ISG is a fracton model and we do not go to an intermediate ISG of stacks of TC. We do this by using a rewinding schedule of the form GBRBGR where the on-site condensation checks as shown in Fig. 22(a) are measured along with the green checks in the G-round. The rewinding schedule ensures that in each round, not all condensation operators evolve into nonlocal stabilizers. The evolution of the condensation operators under the rewinding schedule is shown in Fig. 22. If we had used the schedule GBR, then the R-round will be followed by the G-round and the condensation operators would grow into non-local stabilizers as shown in Fig. 22 and result in an ISG of stacks of toric code. The expected result in the rewinding schedule is that ISGs will be among the fracton model ISGs of the X-cube Floquet code of Ref. [10] since in each round, we have local condensation operators.

## Appendix B: Logical qubits of the 3D Floquet toric code

The counting of logical qubits in the G-ISG is straightforward due to its mapping to the cubic lattice 3D TC up to concatenation with 2-qubit repetition codes. The local relations among plaquette stabilizers on the cubes in the cubic lattice 3D toric code map to the local relation among checks as shown in Fig. 23. Here, we state the counting of logical qubits in the cubic lattice 3D toric code, which implies the same for the G-ISG. On a torus with linear size  $L$ , there are  $3L^3$  physical qubits,  $3L^3$  plaquette stabilizers with  $L^3 - 2$  independent local relations among them,  $L^3$  vertex stabilizers with 1 global relation among them. Thus, we get 3 logical qubits.

For the B-ISG, the evolved condensation operators are either local operators as shown in Fig. 7 or nonlocal stabilizers as shown in Fig. 10. We also have blue-green plaquettes as stabilizers in the ISG. Besides that, we have the stabilizers of the check group and the blue checks as stabilizers of the ISG. It is again useful to work in the effective picture of a 3-foliated stack of 2D rotated TCs and consider the condensation operators and nonlocal stabilizers on top of that. We start with the stack of 2D rotated TCs with periodic boundary conditions and we now have the  $X^{\otimes 4}$  condensation operators in the configuration as shown in Fig. 8(a). On every cube of this lattice, we have a  $Z$  stabilizer as described above i.e., it is the product of  $Z$  stabilizers among three plaquettes sharing the canonical corner associated with the cube. These  $Z$  stabilizers correspond to the vertex operators of the two copies of 3D TCs. We assume the linear system size  $L$  to be even here and in the discussion on automor-

phism below. This is because in the B-ISG, having an odd number of cubes on a torus will lead to a spatial defect in the configuration of condensation terms shown in Fig. 8(a) and we avoid such a scenario for simplicity. There are  $L^3$  cubes and thus  $L^3$  such  $Z$  stabilizer operators. There are two relations among these  $Z$  stabilizers, one on each sublattice, leaving us with  $L^3 - 2$  independent  $Z$  stabilizers. There are  $3L^2$   $X$  plaquette stabilizers and  $3L \times L^2/4$  condensation stabilizers where  $3L$  is the number of planes. The number of relations among the  $X$  stabilizers is  $L^3/4 + 4$ . The form of relations is complicated and is shown in the supplementary **Mathematica** file. Considering the 3 nonlocal stabilizers, we get 3 logical qubits for the B-ISG. The B-ISG can be mapped via an explicit circuit to two copies of 3D TCs up to nonlocal stabilizers; see supplementary **Mathematica** file. The counting of logical qubits in the other ISGs is similar to these the counting for G-ISG or B-ISG.

## Appendix C: Alternative 6-round Floquet color code schedule

In this appendix, we specify a variant of the Floquet color code that exhibits a trivial automorphism of the logical operator representations. The schedule is depicted in Fig. 24. This schedule is designed so that the hexagon and inflated hexagon stabilizers of the blue plaquettes can be inferred from rounds 0 and 1. Similarly, the stabilizers associated with the green and red hexagons and inflated hexagons can be inferred from the 2,3 and 4,5 measurement rounds, respectively.

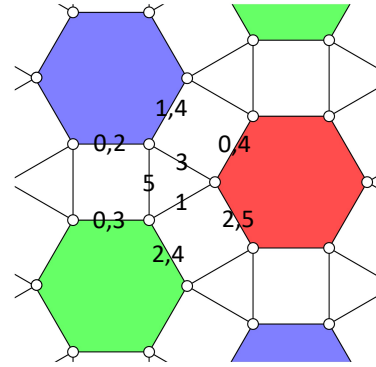


FIG. 24. 6-round schedule that has the trivial automorphism of dynamically generated logical operators.

The ISGs after rounds 0 and 1 are shown in Fig. 25. The ISGs for rounds 2,3,4,5 can be determined by applying the lattice symmetries. Using entanglement renormalization, we find that each ISG is FDLQC-equivalent to the color code. The explicit FDLQCs, written using the polynomial representation [30, 38], can be found in the supplementary **Mathematica** files [39].



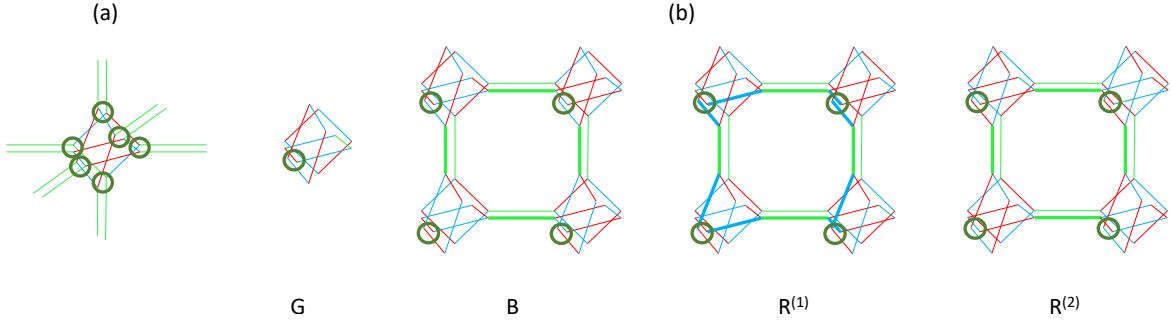


FIG. 22. (a) Two-qubit condensation checks (green round) in the X-cube Floquet code (b) The evolution of one condensation operator in the Floquet code with schedule  $\text{GBR}^{(1)}\text{BGR}^{(2)}$ . The different rounds are labeled. There is no difference in the ISGs in the two B-rounds and in the two G-rounds respectively due to rewinding.

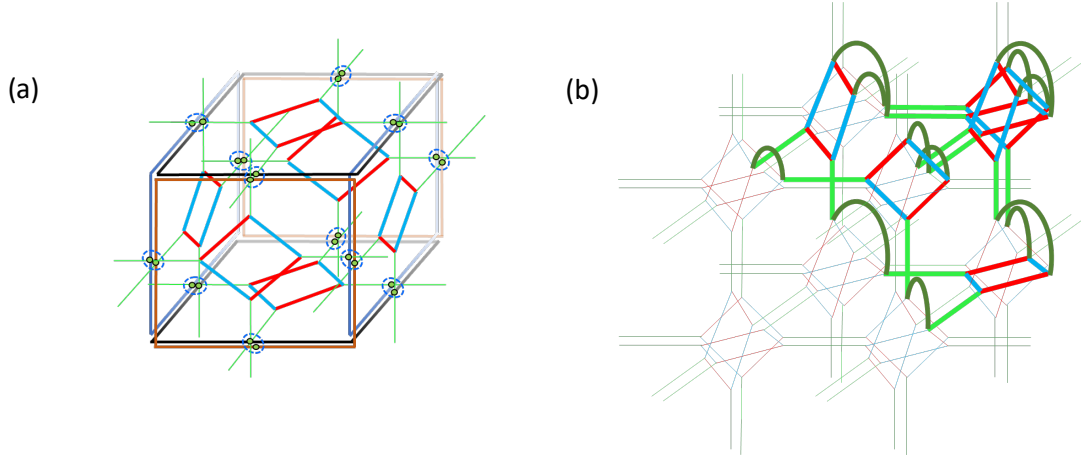


FIG. 23. (a) A local relation in the 3D TC stabilizer group obtained from condensation in stacks of square lattice TC; the product of the  $ZZZZ$  plaquette operators of 3D TCs on the six plaquettes around a cube and the  $ZZ$  condensation operators on the encircled pairs of qubits is equal to the identity. To understand the local relation in the G-ISG of the Floquet code, we also show the square octagon plaquettes corresponding to plaquettes involved in the local relation shown in (a). (b) The corresponding local relation in the G-ISG of 3D Floquet TC on the associated lattice (stacks of the 2D square-octagon lattices). It is a product of condensation operators (shown using bold dark green arcs), green checks (shown in bold green), and the square plaquette operators (which are products of red and blue checks highlighted in bold).

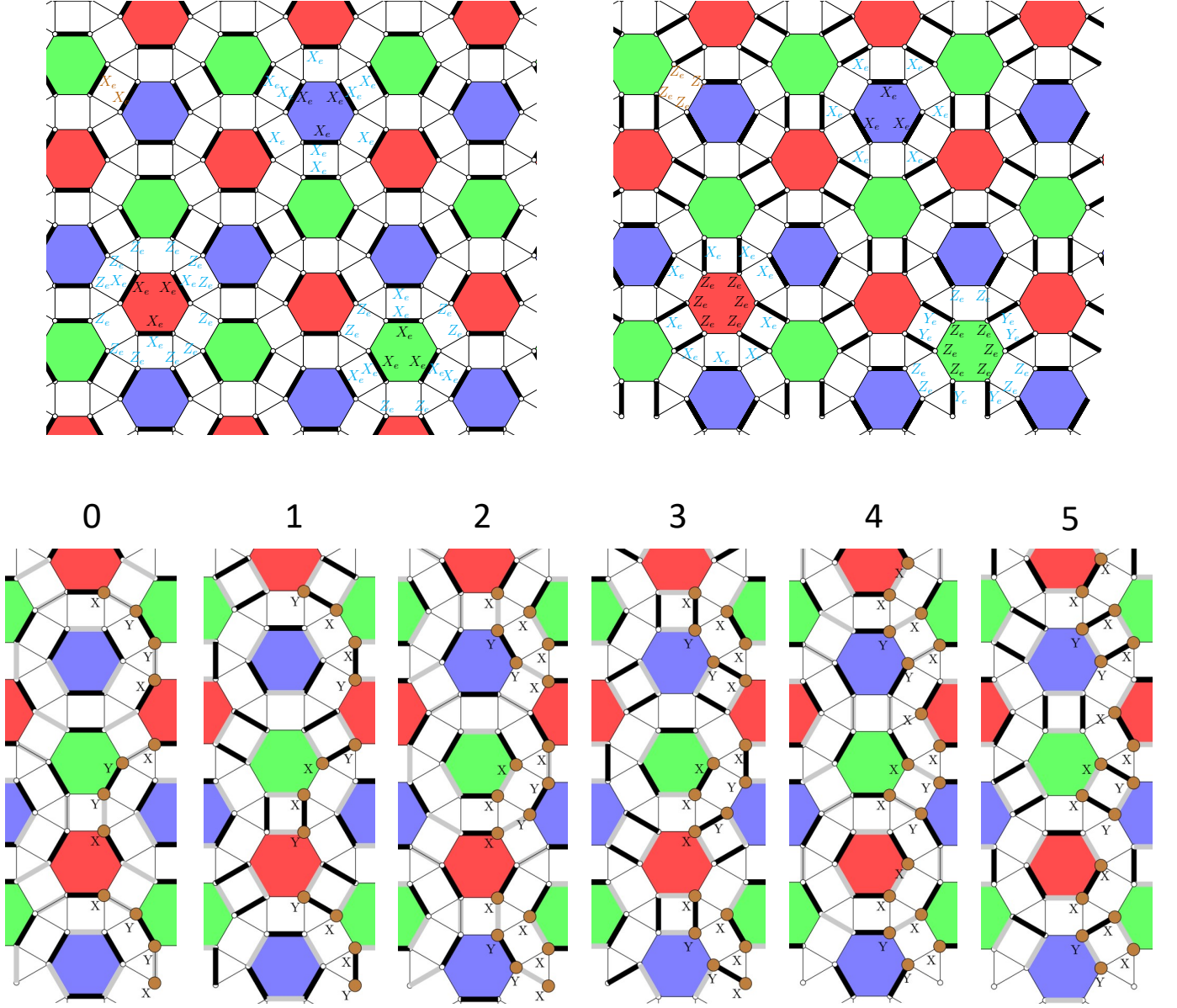


FIG. 25. Top row: Effective color code ISG stabilizers after measurements of round-0 and round-1, respectively, in the six-round Floquet color code with trivial automorphism. The thick black edges indicate the check operators measured in the current round. The six stabilizer generators, two for each inflated hexagon are shown in terms of effective edge logical operators  $X_e$  and  $Z_e$ . On an edge with  $XX$  check,  $X_e = ZZ, Z_e = XI$ , on an edge with  $YY$  check,  $X_e = XX, Z_e = YI$  and on an edge with  $ZZ$  check,  $X_e = XX, Z_e = ZI$ . The inflated hexagon stabilizers are written in cyan color while the hexagon stabilizers are written in black. For round 0, the stabilizer shown in brown is a  $ZZZZ$  operator left invariant from the previous round of measurements and is expressed as  $X_e X_e$  in terms of the effective edge Pauli operators. Right: For round-1, the stabilizer shown in brown is a  $ZZYY$  operator left invariant from the product of  $ZZZZ$  and  $IIXX$  measured in the previous two rounds of measurements; it is expressed as  $Z_e Z_e Z_e Z_e$  in terms of the effective edge Pauli operators. Bottom row: The trivial automorphism of a logical operator in the 6-round Floquet color code. The thick black edges indicate the check operators measured in the current round and the gray edges indicate the checks measured in the next round.